NSSI Neutron Newsletter

Number 2
November 2022

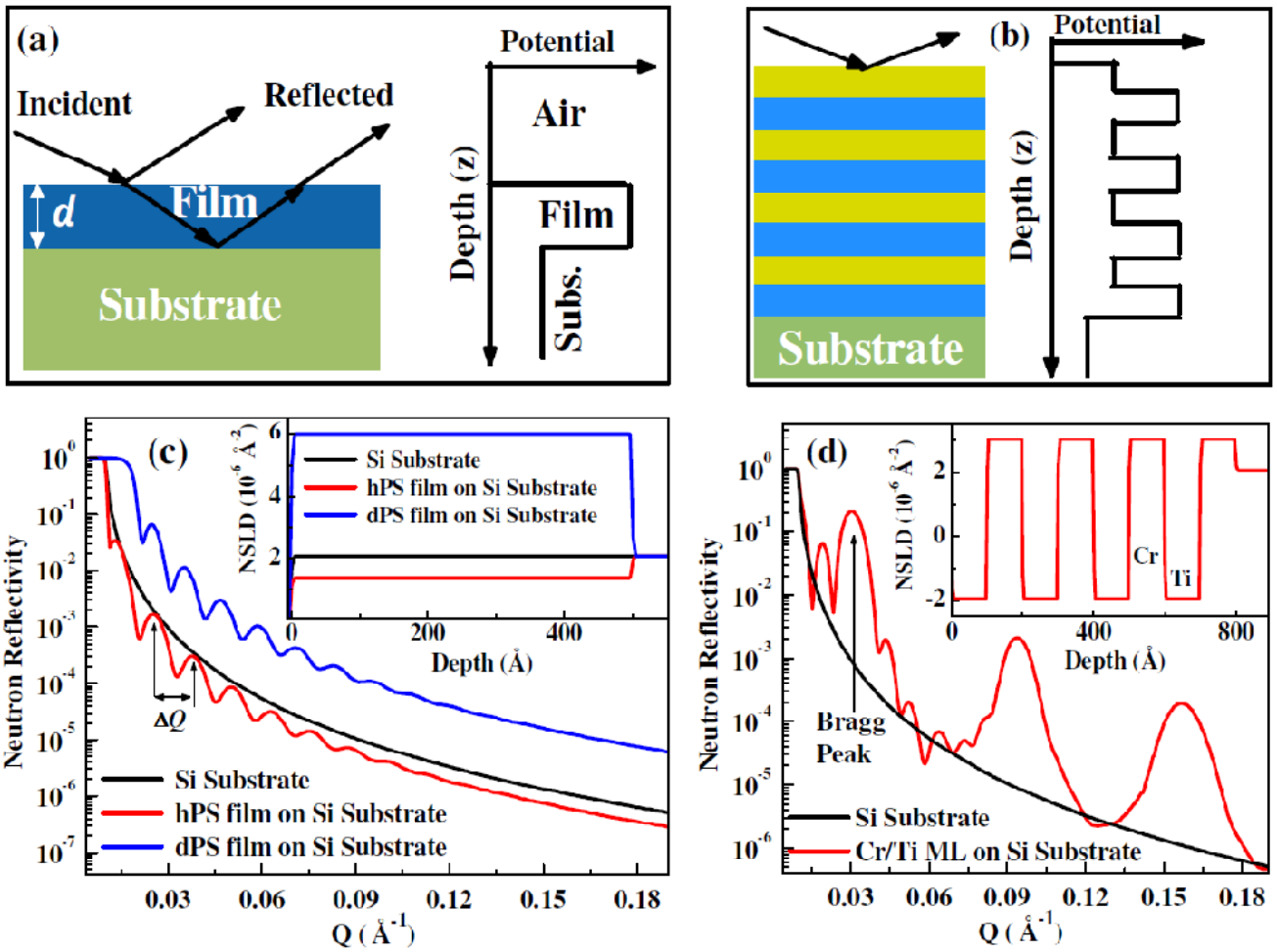

Neutron Scattering Society of India

Neutron Scattering Society of India (NSSI) was formed in 2008 during a meeting of neutron users at Mumbai with an objective to promote the research and development activities of neutron-scattering science and applications. Another aim to form NSSI was to represent the neutron users in the Asia-Oceania Neutron Scattering Association (AONSA), which is an affiliation of neutron scattering societies, which directly represent users in the Asia-Oceania Region. By this NSSI could become one of the founder members of the AONSA along with, Japan, South Korea, Australia and Taiwan. At present NSSI has about 262 registered members from various universities and institutions spread all over the country.

Cover Page

Schematic of neutron reflectivity and depth-dependent potential from a single film and a multilayer grown on a substrate. See the article on Neutron Reflectometry by Surendra Singh (page 18).

Contents

Editorial

The Neutron Scattering Society of India (NSSI) is happy to bring out this NSSI Newsletter in a new format. Besides the Highlights of recent neutron research, as contributed by several NSSI Members, a novel feature is a topical review of an important neutron technique. This issue contains the review of Neutron Reflectometry by Dr. Surendra Singh. The issue also includes the news from the Members and weblinks to upcoming neutron events.

We expect the NSSI Newsletter will be a regular publication of NSSI activities, and welcome contributions from all the Members. The timeline of the next Newsletter will be intimated by email.

We thank all the contributors to this Newsletter.

Published by The General Secretary, NSSI.

Message from the President, NSSI

The Managing Committee of the Neutron Scattering Society of India (NSSI) at its recently held meeting resolved to revive the publication of NSSI Newsletter. In this context, I am delighted to present before you the latest issue of NSSI Newsletter. I take this opportunity to congratulate the Editorial Team for preparing an impressive issue in a rather short period of time. The present issue contains a report of the NSSI for the year 2021 submitted to the AONSA, details related to various instruments at Dhruva, a few selected neutron research highlights, a nice status report on Neutron Reflectivity and news about forthcoming neutron conferences and workshops.

The NSSI was founded nearly 15 years ago for promoting neutron-based research in the country using various instruments at the Dhruva reactor as well as at various international neutron facilities. The NSSI is an affiliate national society of the Asia-Oceania Neutron Scattering Association (AONSA) comprising various national neutron scattering societies in the Asia-Oceania region.At present, NSSI has over 250 registered members from universities, institutes and national R&D institutions spread over the entire country. The actual number of scientists using neutrons as a probe is significantly higher than 250 and it will be our constant endeavour to induct them as Members of the NSSI.

Majority of the experiments at Dhruva reactor are supported financially through the Mumbai Centre of the UGC-DAE Consortium for Scientific Research and BRNS while access to the international neutron facilities are supported through various schemes of the science departments of the Government of India. The NSSI, Mumbai Centre of the UGC-DAE CSR and the Solid State Physics Division have been regularly holding conferences, schools and awareness workshops for the benefit of the existing as well as potential neutron users. Last year, it initiated a "NSSI Special Lecture" series to honour eminent personalities in the field of neutron scattering at one of its national conferences/schools on neutrons. Dr. B.A. Dasannacharya, former Director of the Solid State & Spectroscopy Group, BARC and UGC-DAE-CSR, Indore, and recipient of AONSA Prize 2013, delivered the first NSSI Special Lecture at the 7th Conference on Neutron Scattering (CNS-2021), held at BARC during November, 2021. The second lecture in this series would be delivered by Professor Brendan J. Kennedy, University of Sydney at the XIX School on Neutrons as Probes of Condensed Matter (NPCM-2022) to be held at BARC during November 14-19, 2022.

We sincerely hope that NSSI Newsletter will be published regularly now onwards, at least on yearly basis.I look forward to enthusiastic participation of the NSSI members in terms of short status reports, research highlights and suggestions for the future issues of the Newsletter.

Dhananjai Pandey
President, NSSI

Report from Neutron Scattering Society of India (NSSI)

To promote neutron-based research in the country and to enhance the collaboration among the researchers, the "Conference on Neutron Scattering (CNS)" series conferences, are organized by SSPD, BARC in association with the neutron scattering Society of India (NSSI) in a period of 2-3 years.

The 7th Conference on Neutron Scattering (CNS-2021) was organized in a hybrid mode during November 25-27, 2021 in Mumbai, India to discuss the recent advances in condensed matter physics research by neutron scattering and current developments in neutron facilities. The conference covered all the emerging topics of advances in magnetism, novel techniques, structure and dynamics in supramolecular systems, strongly correlated electron systems, energy materials, mesoscopic systems, and quantum materials. Nearly two hundred contributory abstracts were received and 27 abstracts were selected for oral presentations. There were twenty-five invited talks by the experts covering all the topics of the conference. The organizing committee of the conference was chaired by Dr. S. M. Yusuf, Director, Physics Group, BARC. Dr. Jitendra Bahadur, BARC was the scientific secretary for the conference. The financial support was received from NSSI.

The three-day conference was opened by an inaugural address by Dr. R. Chidambaram, DAE Homi Bhabha Chair Professor and Former Principal Scientific Adviser, Government of India & Former Chairman, Atomic Energy Commission, India. Dr. S. M. Yusuf welcomed the delegates and provided a brief overview of the neutron scattering activities in India. Dr. Yusuf informed that neutron scattering activities in the country are expected to grow manifold with the advanced instruments being planned at the proposed High Flux Research Reactor, BARC (Vizag), India. Invited talks were given by delegates from India as well as from the Asia-Oceania region.

The sessions of the conference were chaired by eminent subject experts. The discussions after each talk were vibrant and exciting, which benefited participants including the students. The conference was rounded out by the distinction of young scientists including PhD students, post-docs, and early-career scientists for their excellent research and their presentations. The conference also had impressive short presentations and more than 100poster presentations.

Another important event organized during the CNS-2021 was 1stNSSI lecture delivered by Dr. B. A. Dasannacharya (the recipient of AONSA Prize 2013) who contributed immensely to neutron scattering research in India, through his early development of neutron spectroscopy and its applications for the dynamics in low-temperature liquids and molecular solids. Dr. B. A. Dasannacharya was felicitated by a medal and a citation.

The conference led to a multitude of inspiring and fruitful discussions with a strong outlook towards the perspective of neutron scattering research to tackle the challenging problems in fundamental and applied research.

(Top) Group photo of the participants attending the conference in physical mode

(Bottom) Left: Inauguration of the conference by Dr. R. Chidambaram, DAE Homi Bhabha Chair Professor and Former Principal Scientific Adviser, Government of India & Former Chairman, Atomic Energy Commission, India. **Right**: Felicitation of Dr. B. A. Dasannacharya during 1st NSSI lecture on neutron scattering.

S. M. Yusuf
Neutron Scattering Society of India

Highlights of Neutron Research

A Methodological Advancement in Estimating Packing Fraction of Correlated Nano-Ellipsoids from Small-Angle Scattering

The packing of particles inside a finite space is ubiquitous. It becomes more fascinating when particles deviate from spherical symmetry. In case of shape-anisotropic particles, rotational degrees of freedom play a crucial role in their positional arrangements and that substantially complicates the jamming characteristics, particularly in a strongly correlated system. The jamming behaviour of anisotropic particles, especially in nanometric length scales, has significant relevance to several practical problems in condensed matter and biological systems. In order to understand the jamming characteristic of a densely packed system, one needs to evaluate the positional correlations of the jammed particles and quantitatively estimate the packing fraction. A novel approach is formulated [1] to determine the packing fraction of jammed nano-ellipsoids in a microsphere by accessing a wide wave-vector transfer (Q) range using medium resolution small-angle neutron scattering (MSANS) and small-angle X-ray scattering (SAXS) data. The method has been elucidated through a quantitative analysis of structural correlation of nano hematite ellipsoids, which were packed in the form of a 3D microgranule using rapid evaporative assembly. The conventional analysis of scattering data misleads to erroneous estimation of packing fraction because of smearing out of the structural correlation by orientation distribution among the ellipsoids. This anomaly in the estimation of packing fraction is overcome by evaluating an inter-particle distance distribution function of jammed nano-ellipsoids. The figures below show micro-granule comprised of jammed ellipsoids and the combined MSANS/SAXS data and an illustration of evaluating the inter-particle distance distribution function of jammed ellipsoids, respectively.

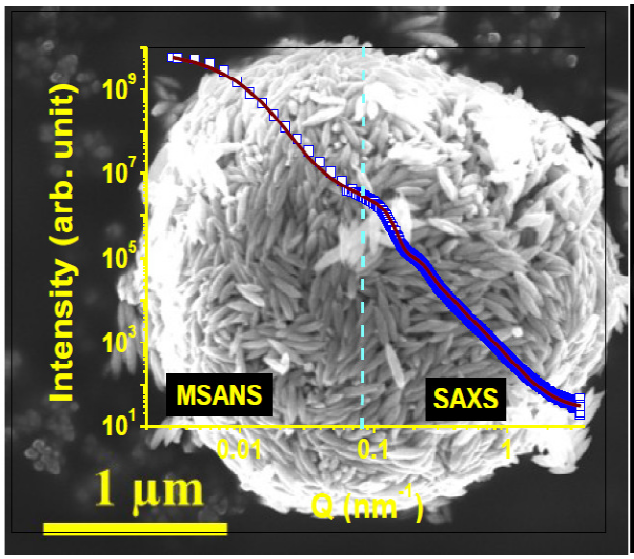

Fig. 1. Scanning electron micrograph and combined MSANS-SAXS profile of micro-granule comprised of highly correlated hematite nano-ellipsoids synthesized by evaporative assembly.

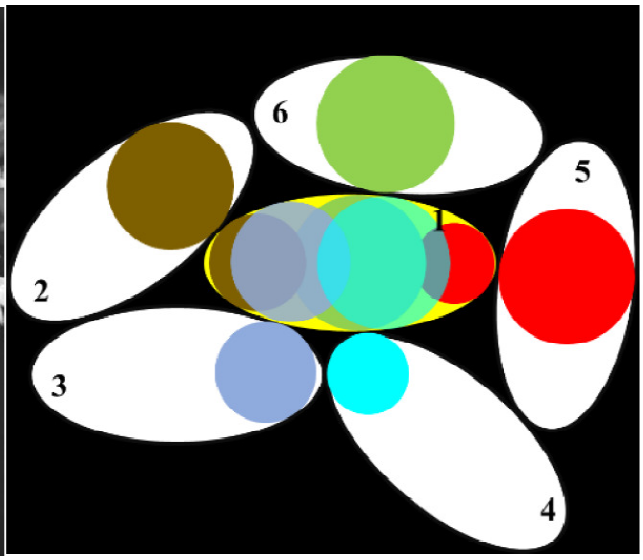

Fig. 2. An illustration demonstrating the effective structural correlation between ellipsoids by considering inscribed spheres which are in contact of neighboring ellipsoids. Ellipsoids-1 and 5 interact via red spheres and so on.

1. *Jamming of Nano-Ellipsoids in a Microsphere: A Quantitative Analysis of Packing Fraction by Small-Angle Scattering*, Avik Das, Ranajit Mondal, Debasis Sen, Jitendra Bahadur, Dillip K. Satapathy and Madivala G. Basavaraj, *Langmuir* **38**, 3832 (2022).

Contibuted by: Debasis Sen, BARC, Mumbai (Email: debasis@barc.gov.in)

Neutron-Irradiation Induced Magnetization and Persistent Defects at High Temperatures in Graphite

Structural as well as magnetization studies have been carried out on graphite samples irradiated by neutrons over 50 years in the CIRUS research reactor at Trombay. Our studies performed on irradiated graphite samples are also applicable to other graphitic materials such as graphene and carbon nanotubes which have a similar two-dimensional layered structure.

Neutron diffraction studies on irradiated graphite samples show (Fig. 1(a)) that the static disorder along the c-axis of the graphite hexagonal structure persists at high temperatures much above the temperature of release of the Wigner energy (653 K). The persistence of the defects at high temperatures has important consequences for the application of graphitic materials in high radiation environments. The magnetization experiments reveal (Fig. 1(b)) weak ferromagnetism at 300 K that persists up to 850 K, and also a large paramagnetic contribution. The Electron spin resonance experiments have been performed to show that irradiation may have broken many chemical bonds resulting in significant number of unpaired spins.

Ab-initio spin-polarized density-functional calculations are performed to understand the origin of magnetism in irradiated graphite, which show that the magnetism arises on one of the 2-coordinated carbon atoms in the region around a vacancy. Our experimental observation of magnetism in defected graphitic materials is of fundamental importance as these materials find wide applications.

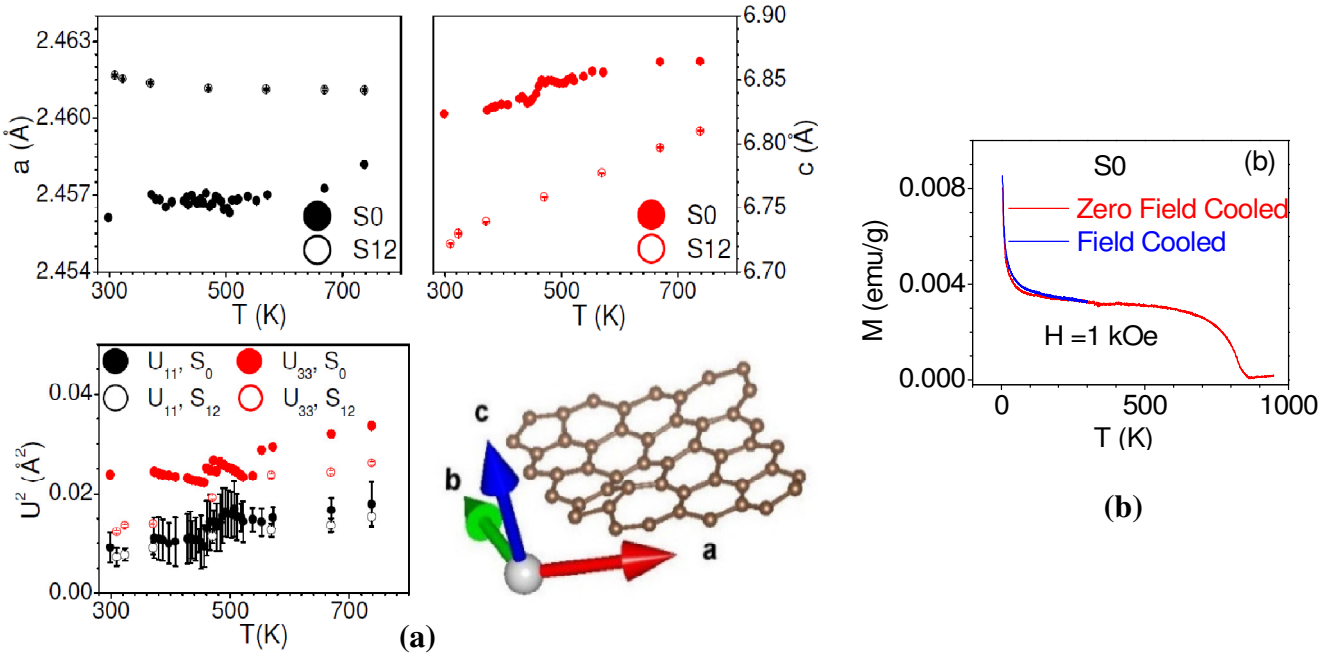

Fig. 1(a). The temperature variation of the lattice and thermal parameters of irradiated (S0) and unirradiated (S12) graphite as obtained from Rietveld analyses of neutron diffraction data. The parameters of the two samples continue to differ beyond 653 K (see text). We show a simulated structure with a persistent defect, namely, an intralayer Frenkel defect consisting of five- and seven-member carbon rings at 900 K**(b)** The variation of Zero-Field-Cooled and Field-Cooled magnetizations with temperature.

1. *Neutron-Irradiation Induced Magnetization and Persistent Defects at High Temperatures in Graphite*, R. Mittal, M. K. Gupta, S. K. Mishra, S.Wajhal, P. D, Babu, M, Mohapatra, B. Singh, A. B. Shinde, P. S. R. Krishna, R. M. Kadam, R. K. Singhal, R. Ranjan and S. L. Chaplot, Phys. Rev. B **105**, 104106 (2022)

Contibuted by: R. Mittal, BARC, Mumbai (Email: rmittal@barc.gov.in)

Insight of negative magnetization, exchange-bias, and electrical properties of $La_{1-x}Pr_xCrO_3$through neutron diffraction and depolarization studies

Technologically important phenomenon of negative magnetization (NM) has been observed in $La_{1-x}Pr_xCrO_3$(x = 0.25, 0.5, and 0.75) compounds [Fig.1(a)]. Further, these compounds exhibit NM along with positive EB, indicating a correlation between these two properties. We have studied the ordering of the involved magnetic sublattices and the net moment variation as a function of temperature by employing neutron diffraction and depolarization techniques. The increasing neutron beam depolarization with Pr (x) in the depolarization experiment provides evidence of increasing domain magnetization [1] due to uncompensated Cr^{3+} and polarized Pr^{3+} moments. The G-type antiferromagnetic (AFM) orderingCr^{3+} moment for x = 0.25, 0.5, 0.75, and 1compounds is inferred from the neutron diffraction study [Fig.1(b)]. The lattice constants a and c show a crossover at ~ x = 0.75 [inset of Fig. 1(b)] that is correlated to the maximum conductivity and the sign change of exchange-bias at ~ x = 0.75.The NM phenomenon in these compounds has been explained within the framework of Cooke's model where the dominance of antiparallelly coupled polarized Pr^{3+}moment over uncompensated canted AFM Cr^{3+} moment increases below the compensation temperature (T_{COMP}) leading to the NM in these compounds [1].

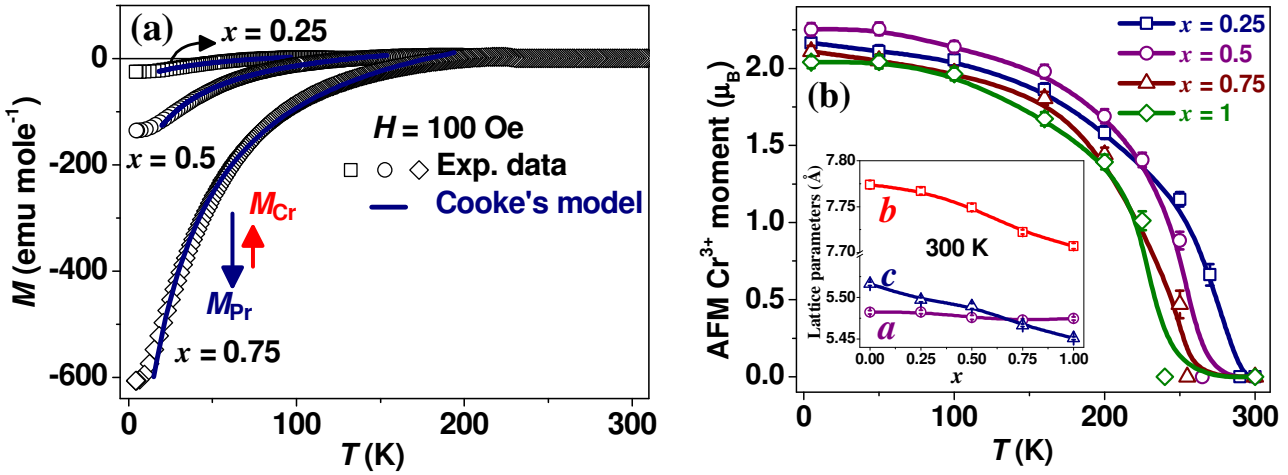

Fig.1 (a) The experimental dc magnetization data (open black symbols) of x = 0.25, 0.5, and 0.75 compounds and their fitting using Cooke's model (navy-blue curve). (b) Thermal variation of AFMCr^{3+}moment. Inset shows the composition dependence of lattice parameters, derived from the neutron diffraction, at 300 K.

1. *Correlated negative magnetization, exchange bias, and electrical properties in La1-xPrxCrO3*, Deepak, Amit Kumar, A. K. Bera, and S. M. Yusuf, Phys. Rev. Mater. **6**, 074405, 2022.

Contibuted by: Amit Kumar, BARC, Mumbai (Email: amitkr@barc.gov.in)

Magnetism of the 2D honeycomb layered $Na_2Ni_2TeO_6$ compound driven by intermediate Na-layer crystal-structure

Magnetism of a compound normally depends on the symmetry of magnetic ions/atoms in the crystal and the nature of exchange interaction between them. However, there are few rare cases where the magnetic symmetry depends on the symmetry of the nonmagnetic ions. Here, we present such a case, investigated by neutron diffraction and inelastic neutron scattering, where the magnetism of the 2D honeycomb layered $Na_2Ni_2TeO_6$ compound is driven by the symmetry of the intermediate non-magnetic Na-layers. The Na-layers contains chiral nuclear density distributions of Na ions and are resided in between the magnetic layers of Ni^{2+} ion (S=1) with honeycomb lattice geometry along the *c* axis. The chirality of the alternating Na layers is opposite. Such alternating chirality of the Na layer dictates the magnetic periodicity along the *c* axis where an up-up-down-down (↑↑↓↓) spin arrangement of the in-plane zigzag AFM structure [characterized by the propagation vector $\boldsymbol{k}$ = (½ ½ ½)] is found. Our results, thus, provide a rare example of magnetic compound where the magnetism is driven by nonmagnetic Na-layers. Besides, the above described commensurate (CM) zigzag AFM order state is found to coexist with an incommensurate (ICM) AFM state below the T_N ~ 27.5 K. The ICM state is found to appear at much higher temperature ~ 50 K and persists down to lowest measured temperature of 1.7 K. Our reverse Monte Carlo (RMC) analysis divulges a two dimensional (2D) magnetic correlations (within the *ab* plane) of the ICM AFM state over the entire temperature range 1.7-50 K. Further, the spin-Hamiltonian, determined by inelastic neutron scattering and subsequent linear spin-wave theory analysis, reveals the presence of competing inplane exchange interactions up to 3rd nearest neighbours consistent with the zigzag AFM ground state, and weak interplanar interaction as well as a weak single-ion-anisotropy. The present study divulges the intertwining magneto-structural correlations.

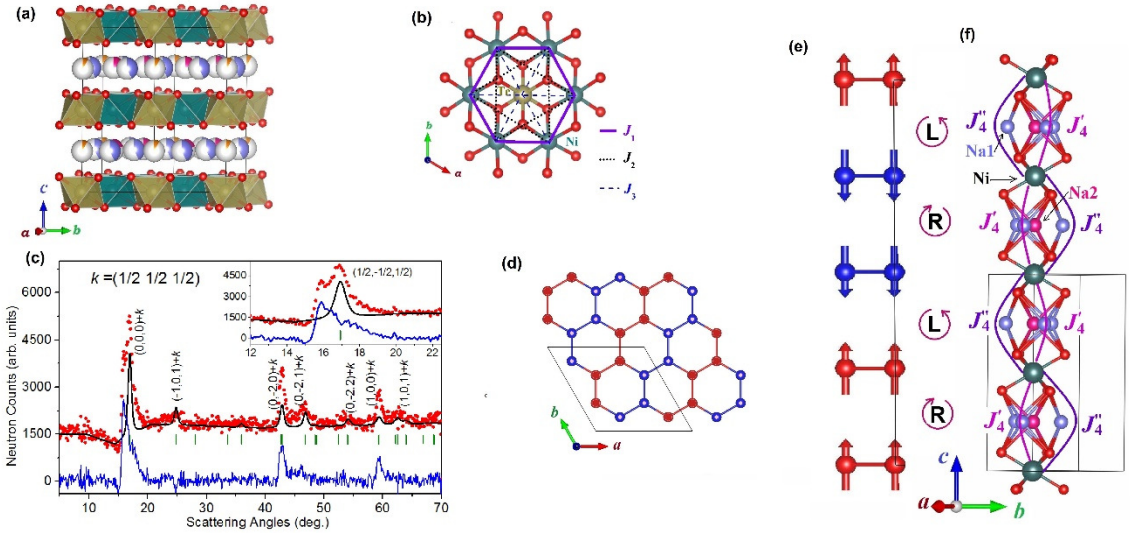

Figure. (a) The layered crystal structure of $Na_2Ni_2TeO_6$. (b) The Honeycomb arrangement of the magnetic Ni^{2+} ions within the ab plane. (c) The pure magnetic diffraction patter at 1.7 K after subtraction of nuclear background measured at 30 K. (d) the zigzag antiferromagnetic ordering within the honeycomb planes (ab-planes). (e) The UUDD spin arrangement along the c-axis. (f) The chiral arrangements of the intermediate NaO layers.

1. *Magnetism of two-dimensional honeycomb layered Na2Ni2TeO6 driven by intermediate Na-layer crystal structure*, A. K. Bera, S. M. Yusuf, L. Keller, F. Yokaichiya, and J. R. Stewart, Phys. Rev. B **105**, 014410, (2022).

Contibuted by: A.K. Bera, BARC, Mumbai (Email: akbera@barc.gov.in)

Experimental observation of emergent many-body composite excitations

The magnetism in one-dimension (1D), dominated by quantum fluctuations, remains one of the extraordinary fundamental topic over the last century and has been explored extensively since the early days of quantum mechanics. Famous Bethe ansatz and its further extensions successfully predict the ground state as well as the excitations of the many-body interactions of the generalized 1D anisotropic Heisenberg–Ising (or XXZ) antiferromagnetic (AFM) chain model. Where, the quasiparticle spinon excitations with fractional quantum numberspin-1/2, as well as many body Bethe string states have subsequently been accurately calculated and precisely verified experimentally. However, the utility of the Bethe ansatz is limited when perturbing the AFM chain model beyond the solvable uniform XXZ model, such as, with the periodic exchange interactions within the chain. One of such models is a quantum trimer spin-chain with repeating couplings J_1-J_1-J_2 (intratrimer J_1, and intertrimer J_2) [Fig. (a-b)] for which emergent composite excitations of novel quasi-particles *doublons* and *quartons*[Fig. (c)], in addition to the low energy fractional spinon excitations, have been theoretically predicted very recently. Our recent neutron scattering study on the model spin-1/2 trimer-chain antiferromagnet $Na_2Cu_3Ge_4O_{12}$ provides the first experimental realization of such emergent composite excitations of the novel quasi-particles, *doublons* and *quartons* [Fig. (d)], as well as their full characterizations in terms of the characteristic energies, dispersion relations, and dynamical structure factor. The present study thus highlights quantum many-body physics beyond the Bethe ansatz.

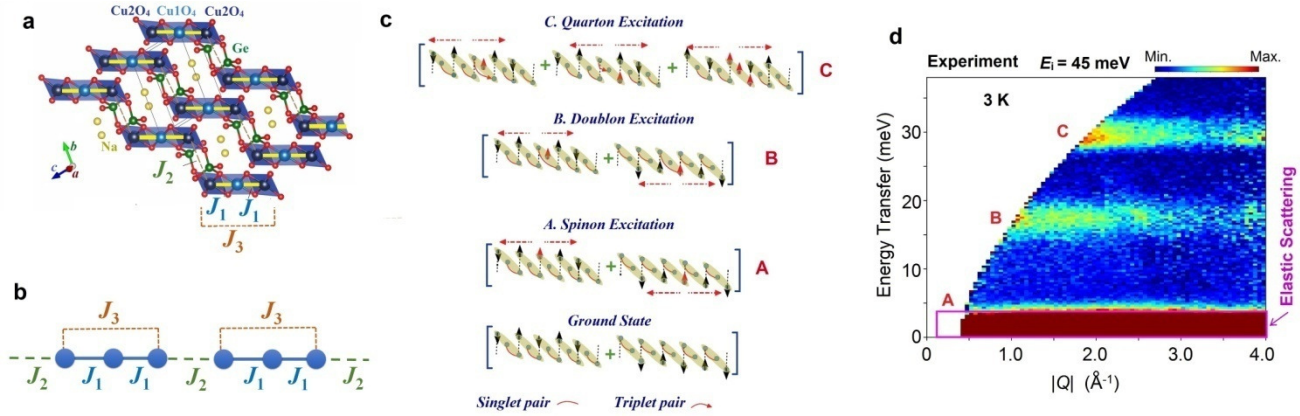

Figure: (a) The crystal structure of $Na_2Cu_3Ge_4O_{12}$. (b) A schematic of a weakly coupled trimer-chain model with J_1, J_2 and J_3 are being NN intratrimer, NN intertrimer and NNN intratrimer exchange interactions. (c) The possible spin configurations for the ground state and the excitation states (spinon, doublon and quarton excitations) of a spin-1/2 trimer-chain model. The red arrows are the flipped spins with respected to the ground state. Red dashed arrows show the delocalization of spins throughout the system. (d) The experimentally measures inelastic neutron scattering (INS) spectrum at T = 3 K using a fixed incident energy of E_i = 45 meV. The intensities are denoted by different colours, as indicated by the scale.

1. *Emergent many-body composite excitations of interacting spin-1/2 trimers*, A. K. Bera, S. M. Yusuf, S. K. Saha, M. Kumar, D. Voneshen, Y. Skourski, and S. A. Zvyagin, *Nature Communications* (2022, in press).

Contibuted by: A.K. Bera, BARC, Mumbai (Email: akbera@barc.gov.in)

Multivalent Ion-induced Control of Self-Assembly in Soft Matter

The effect of the multivalent ions on the self-assembly of three surfactants (amphiphilic molecules), namely, anionic sodium dodecyl sulfate (SDS), nonionic decaoxyethylene n-dodecylether ($C_{12}E_{10}$), and cationic dodecyltrimethyl ammonium bromide (DTAB) has been examined for their interaction with nanoparticles [1]. It is shown that presence of the tetravalent salt $ZrCl_4$ gives rise to almost immediate phase separation of the anionic SDS solution, due to strong condensation of tetravalent counter-ions. This is not consistent with the behavior of the monovalent (NaCl) ions which lead to the structural transitions in the self-assembly. The addition of tetravalent does not give rise to any significant changes in the self-assembly of cationic DTAB and non-ionic surfactant, as it is the Cl^- (monovalent) ions only, which play the role of counter-ions. However, the interaction of these surfactants with anionic silica nanoparticles (HS40) is very different in the absence and presence of multivalent salt. The stable one-phase system of nanoparticles-SDS transforms into a two-phase, whereas nanoparticle-DTAB system which is in two-phase becomes stable (one-phase), in the presence of $ZrCl_4$. Even interesting results are observed with the nanoparticle and non-ionic surfactant system, which undergoes transformation from a stable micelle-decorated one-phase to a two-phase system with increasing $ZrCl_4$ concentration.

The modifications in the phase behavior are explained by interplay of underlying interactions in the system as investigated using small-angle neutron scattering. The nanoparticles undergo a charge reversal due to strong condensation of Zr^{4+}, making nanoparticles anionic to cationic. The nanoparticle interaction with anionic SDS is now driven by electrostatic attraction, whereas by electrostatic repulsion for DTAB micelles. The presence of $ZrCl_4$ gives rise to non-adsorption of the $C_{12}E_{10}$ micelles which in turn causes micelle-driven depletion attraction between nanoparticles and hence nanoparticle aggregation (two-phase).Overall, the study present pathways (Fig. 1) to tune the self-assembly of the amphiphilic molecules and their interactions with nanoparticles, using multivalent ions.

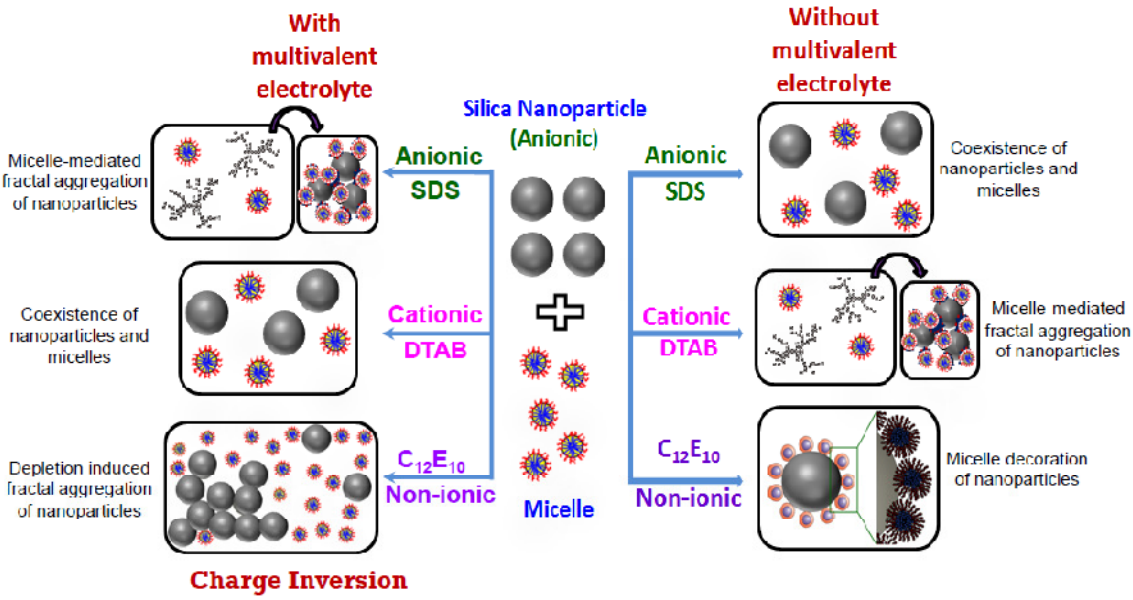

Fig. 1. Schematic illustrating the changes in the phase behavior and evolution of microstructures in nanoparticle-surfactant systems in the absence and presence of multivalent (Zr^{+4}) ions.

1. *Modifications in surfactant-dependent phase behavior of colloidal nanoparticles under charge reversal*, D. Ray, S. Kumar, D. Saha and V. K. Aswal, Chem. Phys. Lett. **799**, 139635 (2022).

Contibuted by: Debes Ray, BARC, Mumbai (Email: debes@barc.gov.in)

Magnetic Proximity Effect in Superconducting/Ferromagnetic complex oxide heterostructures

The magnetic proximity effect (MPE) in superconductor (SC)/ferromagnet(FM) and SC/Insulator(I)/FM hybrid oxide systems has attracted considerable interest due to the emergence of magnetic phases such as the induced magnetically dead/depleted (MD) layer and magnetization reversal, in the FM layer near the interface below the SC transition temperature (*T*sc). The effect of the stacking sequence on magnetic and superconducting properties in both proximity geometry (FM and SC layers in direct contact, S1: $La_{0.67}Sr_{0.33}MnO_3$ (LSMO)/$YBa_2Cu_3O_{7-\delta}$ (YBCO)) and in tunnelling geometry (FM and SC layers are separated by insulating layer, S2: LSMO/$SrTiO_3$/YBCO), which consequently affected the MPE, was investigated using spin-polarized neutron reflectivity (PNR) experiments [1]. The PNR results for S1 and S2 are summarised in the Fig. 1, where depth dependent magnetic scattering length density (MSLD) profiles show emergence of MD layer below *T*sc of YBCO for both the heterostructures. The strength of MPE in these heterostructures was gauged by the thickness of the emergent interfacial MD layer. We found an increase in the *T*sc and magnetization for both the heterostructures (S1, S2) as compared to similarly grown heterostructures with a reversed layer stacking order (S3, S4). The evolution of magnetization of the interfacial FM layer, studied as a function of temperature for both the sets of heterostructure systems (S1, S2 and S3, S4), showed a decrease in the MPE-induced MD layer thickness for heterostructures having a higher *T*sc. Our results established the intrinsic nature of MPE and its correlation with stacking sequence-dependent magnetic and superconducting properties in these heterostructure systems. The long range MPE observed in these systems is attributed to tunnelling of spin triplet cooper pairs from SC to FM layer near the interface. We also established that superconductivity is essential for the existence of MPE in these systems. This was done by suppressing the superconductivity of SC layer by ion irradiation which caused structural changes (evident from XRD) and led to vanishing of MPE. A comparison of the results of different studies with these results suggest that the average magnetization and transition temperatures of a FM and SC are important parameters that dictate the strength of the MPE due to the complex interaction of SC and FM order parameters.

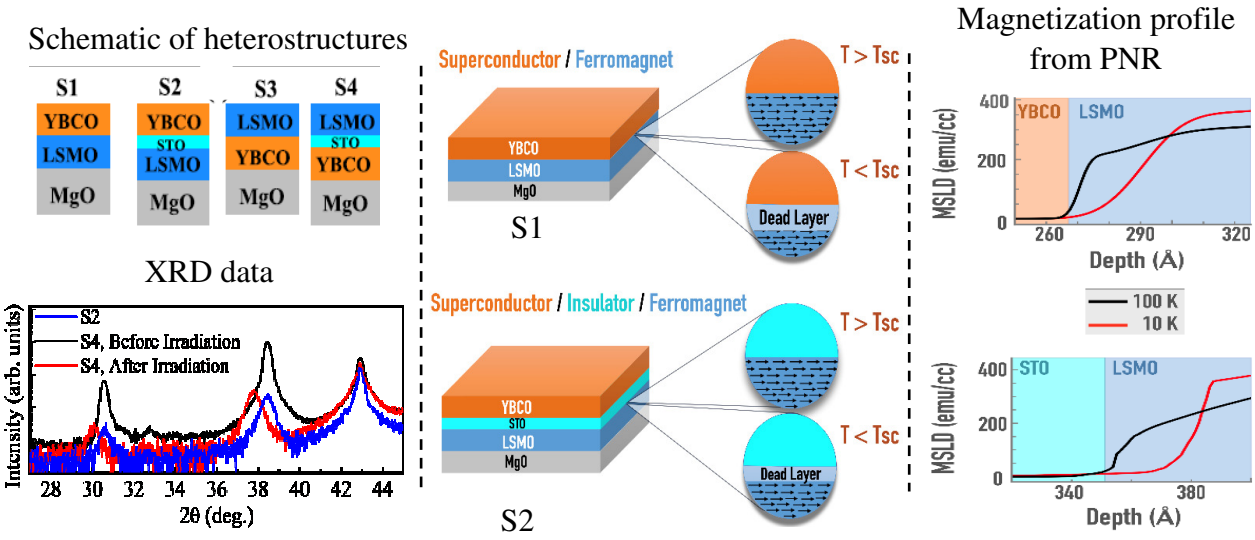

Figure: Left panel shows the schematic of the heterostructures in proximity (S1, S3) and tunnelling geometry (S2, S4), as well as XRD data. The middle panel shows emergence of interfacial MD layer below Tsc. The panel on right shows depth dependent MSLD profiles above and below Tsc for S1 and S2 indicating emergence of MD layer at the interface below Tsc.

1. *Correlation of Magnetic and Superconducting Properties with the Strength of the Magnetic Proximity Effect in La0. 67Sr0. 33MnO3/SrTiO3/YBa2Cu3O7− δ Heterostructures*, H. Bhatt, Y. Kumar, C. L. Prajapat, C. J Kinane, A. Caruana, S. Langridge, S. Basu, and S. Singh, ACS Appl. Mat. Inter. **14**, 8565 (2022)

Contibuted by: Surendra Singh, BARC, Mumbai (Email: surendra@barc.gov.in)

Understanding Solid Electrolyte Polymer using Neutron Scattering

Solid polymer electrolytes (SPEs) have attracted lot of scientific attention in the recent years due to favorable characteristics such as higher thermal stability and higher safety when compared to liquid polymer electrolytes. Understanding the polymer dynamics and conductivity in polymer electrolytes is essential to develop SPEs that have commercial value. In depth analysis of the microstructural modifications is rare. To accomplish this challenging task we use Small Angle Neutron Scattering (SANS) measurements at BARC. We also use broadband dielectric relaxation spectroscopy (DRS) to understand the polymer dynamics such as relaxation and the transport of ions in the SPEs. Uisng broadband dielectric relaxation spectroscopy we have shown that metacomposite can be formed as graphene concentration is increased in chitosan films [1]. Using SANS, we have shown that graphene assembles as fractals in chitosan films. We have also observed that incorporation of silver nitrate in the films can enhance the metamaterial characteristics of the nanocomposites.

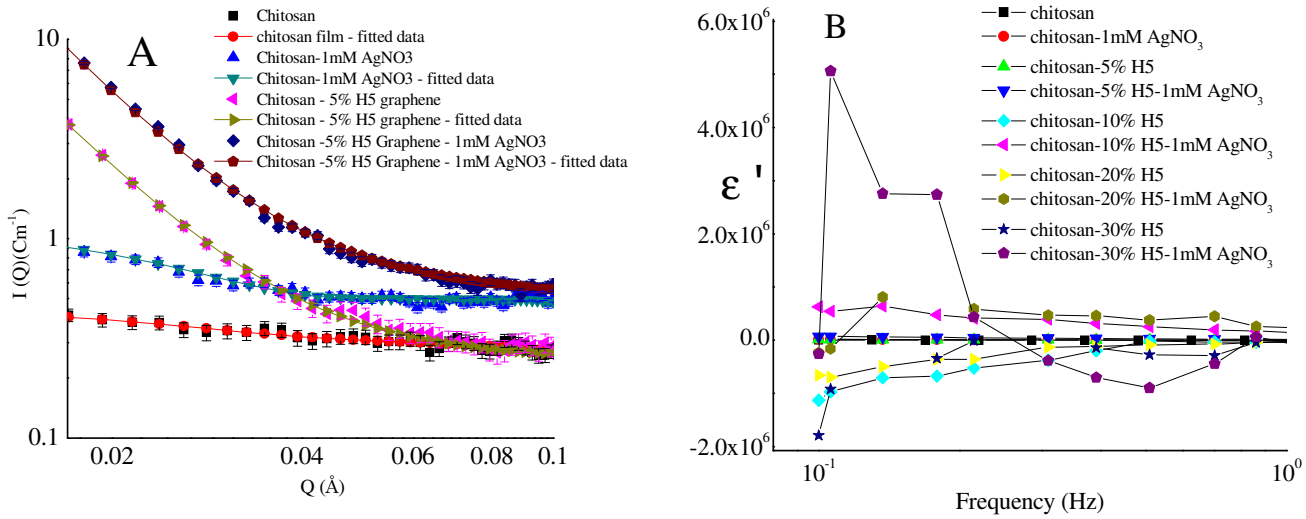

Figures: (A) SANS and (B) Dielectric constant for chitosan-graphene-silver nanocomposites

1. *Broadband dielectric spectroscopy and small-angle neutron scattering investigations of chitosan-graphene-silver metacomposites*, Swathi Somanathan, V. K. Aswal and R. P. Ramasamy. J Mater Sci: Mater Electron **33**, 217 (2022).

Contibuted by: R.P. Ramasamy, Anna University, Chennai (Email: radhaperumalramasamy@gmail.com)

Neutron as a Probe to Understand Therapeutic Actions of Curcumin

Curcumin, the main ingredient in turmeric, an Indian spice, has been touted as a potential candidate for anti-inflammatory, anticancer, wound-healing, and antioxidant properties. It is found as an essential component of different home remedies practised in Indian households. Despite the widespread use of curcumin, its therapeutic action mechanism is not well understood. It has been observed that curcumin alters the function and expression of a wide range of unrelated proteins. However, no preferable binding site of curcumin on any of these proteins has been identified. We have used quasielastic neutron scattering (QENS) to show that curcumin strongly interacts with the lipid membrane and enhances the membrane dynamics. Our study [1] reveals that curcumin preferably locates at the membrane interface which significantly modulates the packing and chain conformation of the lipids resulting alteration in the phase behaviour of the membrane. QENS data reveals that presence of curcumin accelerates the lateral motion of lipids and thereby exercise control over different physiological process such as cell signaling, protein–protein interaction, and functionality of membrane proteins. The observed increase in the lateral motion enhances the membrane fluidity which consequently modulates the functionalities of embedded membrane proteins. Our study supports a possible action mechanism in which curcumin can act as an allosteric regulator of membrane functionality. Hence, transport properties of the lipid membranes could be the key to understanding the science behind the beneficial therapeutic effects of curcumin.

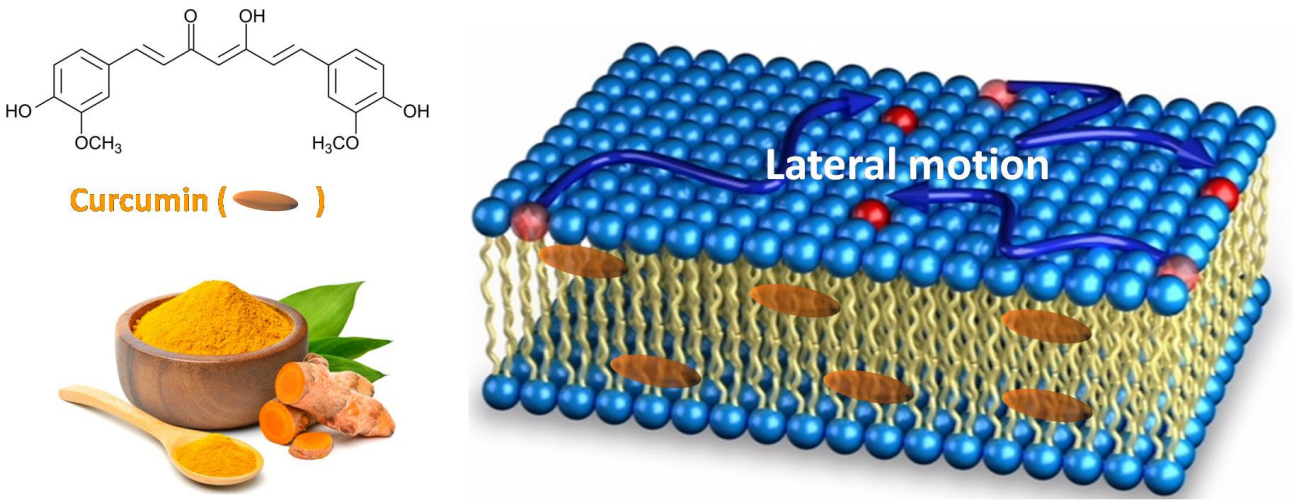

Fig. 1. Schematic of a lipid bilayer with curcumin which is mainly located at the interface of membrane. Lateral motion of lipids within the leaflet is also depicted.

1. *Curcumin Accelerates the Lateral Motion of DPPC Membranes*, V. K. Sharma, J. Gupta, H. Srinivasan, H. Bhatt, S. García Sakai, and S. Mitra, Langmuir **38**, 9649 (2022).

Contibuted by: V.K. Sharma, BARC, Mumbai (Email: sharmavk@barc.gov.in)

Magnetic field dependent neutron diffraction on reduced graphene oxide-$BiFeO_3$ nanocomposite

These days multiferroic compounds are being seen as savior in the quest of achieving extremely high capacity data storage density because of their unique property of coupling between electric and magnetic order parameters which allows switching of magnetization under electric field. A score of compounds are currently being explored and $BiFeO_3$ turns out to be the most promising one because of its room temperature multiferroicity. However, due to large leakage current, the realization of $BiFeO_3$ based four-logic-state multiferroic memory device is still remaining elusive.

Several ways are being tried to find a solution. Development of $BiFeO_3$/graphene nanocomposite is one approach. An interesting nonmonotonic magnetic field dependence of ferroelectric polarization has been observed here. In this work [1], magnetic field dependent neutron powder diffraction (ND) data were recorded for the $BiFeO_3$/reduced-graphene-oxide (BFO/RGO) nanocomposite at the PD-3 diffractometer (wavelength = 1.48 Å). Rietveld refined patterns under zero and 20 kOe magnetic field are plotted in Figs 1 and 2. The data could be fitted with R3c structure while the magnetic structure was found to conform to Γ1 irreducible representation. The parameters such as, magnetic moment, lattice volume, off-centre displacement of the ions (which offers a measure of the ferroelectric polarization) exhibits nonmonotonic magnetic field dependence (Fig 3).

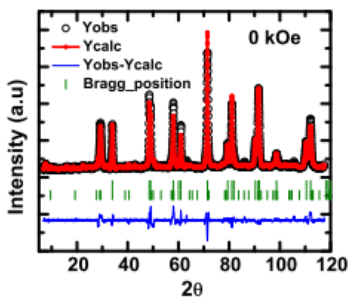

Fig 1: Rietveld refined ND pattern of reduced graphene oxide-BiFeO3 in zero magnetic field.

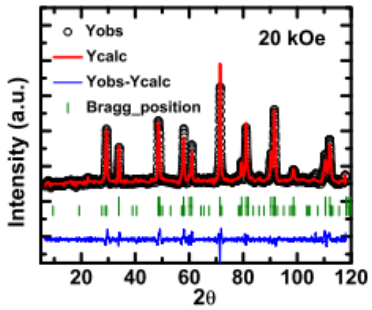

Fig2: Rietveld refined ND pattern of reduced graphene oxide-BiFeO3 in 20kOe.

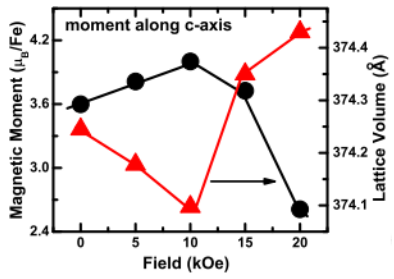

Fig 3: Variation of lattice volume and magnetic moment along c-axis as a function of magnetic field.

In contrast, pure $BiFeO_3$ exhibits negative magnetostriction (both in bulk and nanoscale) and monotonic suppression of polarization under magnetic field. The BFO/RGO nanocomposite, therefore, appears to exhibit both negative and positive magnetostriction at, respectively, bulk and surface regions. Field-dependent competition between the positive and negative magnetostriction results in nonmonotonic magnetic field dependence of polarization. The Fe-C bond at the interface of the nanocomposite possibly plays a significant role in yielding positive magnetostriction. The observed magnetic-field-dependent tuning of ferroelectric polarization (increase or decrease) expands the device application possibility of the BFO/RGO nanocomposite manyfold.

1. *Nonmonotonic Magnetic Field Dependence of RemnantFerroelectric Polarization in Reduced Graphene Oxide–BiFeO3 Nanocomposite,* T. Chatterjee, A. Mukherjee, P. Pal, S. D. Kaushik, V. Siruguri,S. Mandal, S. Hazra, S. Bhattacharjee,C. K.Ghosh, and D. Bhattacharya, Physica Status Solidi RRL **130**, 184101 (2022)

Contibuted by: S.D. Kaushik, UGC-DAE CSR, Mumbai (Email: sdkaushik@csr.res.in)

Small-Angle Scattering probes the structural hierarchy in organized ensembles of nano Zinc Ferrites

Mesoscopic structures in a series of differently organized-ensembles of Zinc Ferrite nanoparticles were investigated. Small-angle scattering provides the quantitative information about the secondary structure and type of hierarchy. Medium-resolution small-angle neutron scattering (MSANS) experiments were performed using a double crystal-based SANS instrument at GT lab, Dhruva reactor, with neutron wavelength ~ 3.12 Å. SANS intensity profiles were analyzed in the light of polydisperse spherical particle model. The size distribution of the particles was extracted from SANS considering the size distribution as lognormal. A series of differently-organized Zinc Ferrite nano-assemblies were considered with isotropic/anisotropic constituent primary nanoparticles [1]. The formation of hierarchy is understood with varied parameters. For the system 'Compact Ensemble of isotropic nanoparticles' (CEIN), the average diameter ($D_{av)}$ is found to be ~190 nm with polydispersity index (σ) of 0.28. In case of 'Compact Ensemble of anisotropic-isotropic nanoparticles' (CEAIN), D_{av} is ~ 205 nm having σ of 0.36. For 'Compact Ensemble of anisotropic nanoparticles' (CE), D_{av} and σ are found to be ~190 nm and 0.23, respectively. While for 'Core-Shell Ensemble' (CSE), the above quantities are found to be ~180 nm and 0.38, for 'Hollow Core Ensemble' (HCE), the $D_{av}$and s are found to be ~195 nm and 0.25, respectively.

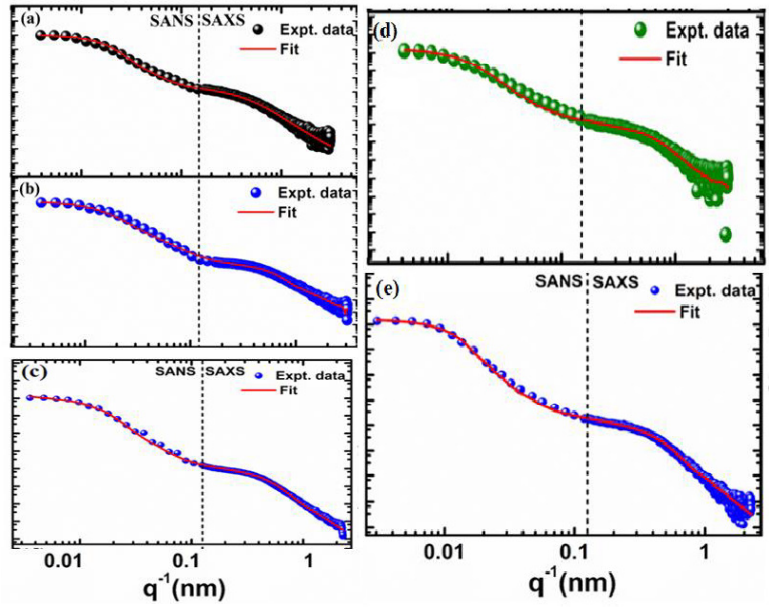

Figure: Combined Small-Angle neutron and X-ray Scattering data along with model fit for (a) CEIN, (b)CEAIN, (c) CE, (d) CSE, (e) HCE samples

1. *Structure-Correlated Magnetic Resonance Transverse Relaxivity Enhancement in Superparamagnetic Ensembles with Complex Anisotropy Landscape*, K. Konwar, N. Sharma, P. Pranjali, A. Guleria, S. D. Kaushik, A. Dutta, R. Mukhopadhyay, D. Sen, W. Gao, and P. Deb, *Langmuir* **38,** 11087 (2022).

Contibuted by: P. Deb, Tezpur University, Tezpur (Email: pdeb@tezu.ernet.in)

A short status review on a Neutron Technique

Neutron Reflectometry: a technique for revealing emergent phenomena at interfaces in heterostructures

Surendra Singh*
Solid State Physics Division, Bhabha Atomic Research Centre, Mumbai 400085 India
&
Homi Bhabha National Institute, Anushaktinagar, Mumbai 400094, India
*Email: surendra@barc.gov.in

Abstract

Neutron reflectometry (NR) has emerged as a unique technique for the investigation of structure and magnetism of thin films of both biologically relevant and magnetic materials. The advantage of NR with respect to many other surface-sensitive techniques is its sub-nanometer resolution that enables structural characterizations at the molecular level. While in the case of bio-relevant samples, NR can be used to probe thin films at buried interfaces, non-destructively, even adopting a complex sample environment. Whereas the polarized version of NR is best suited for revealing the interface magnetism with a sub-nanometer depth resolution. In this article, the basic principle of NR with some applications of NR to both bio-relevant samples and magnetic heterostructures are briefly described.

1 Introduction

Surfaces and interfaces play a crucial role in defining the properties and functionality of both magnetic films[1, 2]and soft matter[3]. Materials at the interface often exhibit peculiar structure and behaviour, which are not observed in their bulk, as it encounters and interacts directly with different materials or phases through a very narrow region of the interface. While there are several practical phenomena relating to our daily life such as adhesion, lubrication, friction, coating, and painting, which are largely attributed to interfacial properties of materials in soft matter, emerging phenomena at interfaces of magnetic heterostructures and thin films attracted much attention for both industrial applications as well as academic researches. In addition, for solving complex biological problems and advancement in the development of highly functionalized biomimetic materials, understanding biological systems at a nanometer resolution is extremely important as many biological processes occur at interfaces in this length scale. Therefore, interface sensitivity has turned out to be the most useful characteristic in studies of magnetic thin films, multilayers, soft matters and biological systems. A wide range of direct and indirect techniques have been developed and used to probe surfaces and interfaces, including optical reflectivity/ellipsometry, optical imaging, fluorescence spectroscopy, surface probe techniques such as atomic force microscopy (AFM) and scanning tunnelling microscope (STM), the electron microscopy probes of the scanning electron microscope (SEM) and transmission electron microscopy (TEM), surface plasmon resonance (SPR), surface sensitive Fourier transform infrared (FTIR) spectroscopy, and X-ray reflectivity (XRR) and neutron reflectivity (NR). Each of these techniques suggests a particular viewpoint on the surface and interfacial properties. However, neutron scattering techniques such as NR offers unique property that makes them powerful techniques for the study of surface and interfaces.

In recent years, XRR and NR have emerged as particularly powerful techniques for probing surface and interfacial structures on a length scale of ~10 to 5000 Å [2].The sensitivity of the NR technique to interfaces is because the projection of the neutron wavelength normal to the surface

matches the thickness of thin films and the neutron wave function becomes strongly distorted near interfaces when the neutron encounters a potential step[2, 4-6]. NR probes the nuclear scattering length density (NSLD) profile perpendicular to the surfaces and interfaces (in contrast to the electron scattering length density, ESLD in XRR), the interface roughness, and the interface morphology[7]. In general, neutron scattering deals with the nuclear interaction of cold/thermal (energy $\leq$ 25 meV) neutrons and the strength of the interaction is characterized by the neutron scattering length, *b*, which varies randomly throughout the periodic table[8]. An important aspect of neutron scattering is that the value of b depends on isotopes and this is especially important for hydrogen (H) and deuterium (D or ^{2}H), which have scattering lengths of different sign and magnitude (*b* values for H and D is -0.374×10^{-12} cm and 0.6674×10^{-12} cm, respectively)[8], thus it can be used to study biological systems. Apart from a few strongly adsorbing elements (e.g. Gd, Sm and Cd), the absorption cross-sections of cold/thermal neutrons are low, suggesting that neutrons are highly penetrating and nondestructive probes. Thus, the NR can probe buried interfaces such as solid/liquid interfaces nondestructively and also can make in situ measurements under various sample environments. In addition, neutrons are unique microscopic probes of magnetism, due to their inherent magnetic moment (μ_N) of ~ -1.913 nuclear magneton (nuclear magneton $=-9.6623647\times10^{-27}$ J/T) that can examine the internal magnetic field (*B*) on the atomic level inside materials. Thus, using polarized NR (PNR) the magnetization depth profile is probed in addition to the nuclear depth profile of magnetic films and heterostructures.

Thus, surfaces and interfaces are present everywhere and the transport of atoms, molecules, or charge across interfaces is fundamentally important to the properties and function of materials. Also, the potential energy gradients at interfaces drive a host of thermodynamic processes. Emerging properties pursued through materials by design will be realized only in new materials having at least one nanoscale dimension e.g. composite materials and heterostructures. New functionality in these systems can arise from interface-dominated forces and interactions, rather than from the less-specific interactions that span the bulk. NR is being used to solve a variety of problems in the field of material science [4, 9, 10], polymers and soft matters [11-13], thin film magnetism[4, 14-19], superconductivity [20-24], chemistry and biology (e.g. surfactants, polymers, lipids, proteins, and mixtures adsorbed at liquid/fluid and solid/fluid interfaces)[25-28]. Here, I will briefly describe the principle of specular (angle of incidence = angle of reflection) neutron reflectivity using a few model systems containing single and multiple interfaces. Also, an experimental procedure with a neutron reflectometer instrument will be described briefly. A typical example of emerging interface magnetism in magnetic heterostructure and soft matter interfaces, where neutron reflectivity has played an important role, will also be described in this review.

2 Neutron Reflectometry

The reflection of light from surfaces, as a result of a change in refractive index, is a well-known phenomenon. Interference of light reflected from the front and back surfaces of the film and optical interference are still used to measure the thickness of surface coatings. During an experiment in the 1920s, Compton showed that X-ray reflection follows the same laws as a reflection of light but with different refractive indices and the refractive index for the X-ray depends on electron number density [29]. In 1944 Fermi and Zinn first demonstrated the mirror reflection of neutrons and neutron reflectivity (NR) measurement for finding out coherent nuclear scattering cross-section of various materials [30]. Most of the neutron scattering techniques, which are now commonplace for studying all branches of basic science and materials, were already well established in the early 1970s but not neutron reflectometry. However, NR emerged and rapidly developed as a dedicated technique in the later 1970s and mid-1980s, for the study of surfaces and interfaces. NR follows the same fundamental equations as optical reflectivity but with different refractive indices. A neutron refractive index of any material depends on the scattering length density of its constituent nuclei and the wavelength of the neutron. The neutron refractive index for

most materials is only slightly less than that of air or vacuum and thus total external reflection is more commonly observed instead of the total internal reflection experienced with light. Over the year neutron reflection has emerged as a powerful technique for investigating the inhomogeneities across the interface like inhomogeneities in composition or magnetization [13, 31].

2.1 Unpolarized Neutron Reflectivity

Unpolarized NR is mostly used to investigate the depth profiling of structure (NSLD depth profiles) of nonmagnetic samples, biophysics and soft matters. This technique is being used for studies of surface chemistry (surfactants, polymers, lipids, proteins and mixtures adsorbed at liquid/fluid and solid/fluid interfaces) and other soft matter interfaces. The non-destructive feature of NR is very helpful to probe bio-relevant thin films at buried interfaces as well as using such samples with bulky sample environment equipment. In addition, the advancement in biomolecular deuteration enabled to probe certain structural features and to accurately resolve the location of chemically similar molecules within a thin film. The schematic geometry of neutron reflectivity is shown in Figure 1. The intensity of the neutron beam reflected at a glancing angle from a flat material surface depends upon the nature of the surface as well as the composition of the underlying matter. Figure 1 shows reflectivity geometry for the two types of possible reflections from a rough surface: (a) Specular reflection: when the angle of incidence (θ_i) is equal to the angle of reflection (θ_f) [$\theta_i = \theta_f = \theta$], and (b) Off-specular scattering: where the above equality is not maintained ($\theta_i \neq \theta_f$). Specifically, specular reflectivity can be analyzed to reconstruct laterally averaged compositional depth profile along the normal to the surface (z-direction in Fig. 1). On the other hand, at the angular position, in which $\theta_i \neq \theta_f$, around the specular reflection position weak off-specular scattering is observed originating from in-plane structures of the sample in the *x*-direction. Experimentally, the specular reflectivity is measured as a function of the momentum transfer wave vector, Q ($= 4\pi \sin\theta/\lambda$ where λ is the wavelength of neutrons), as defined in Fig. 1.

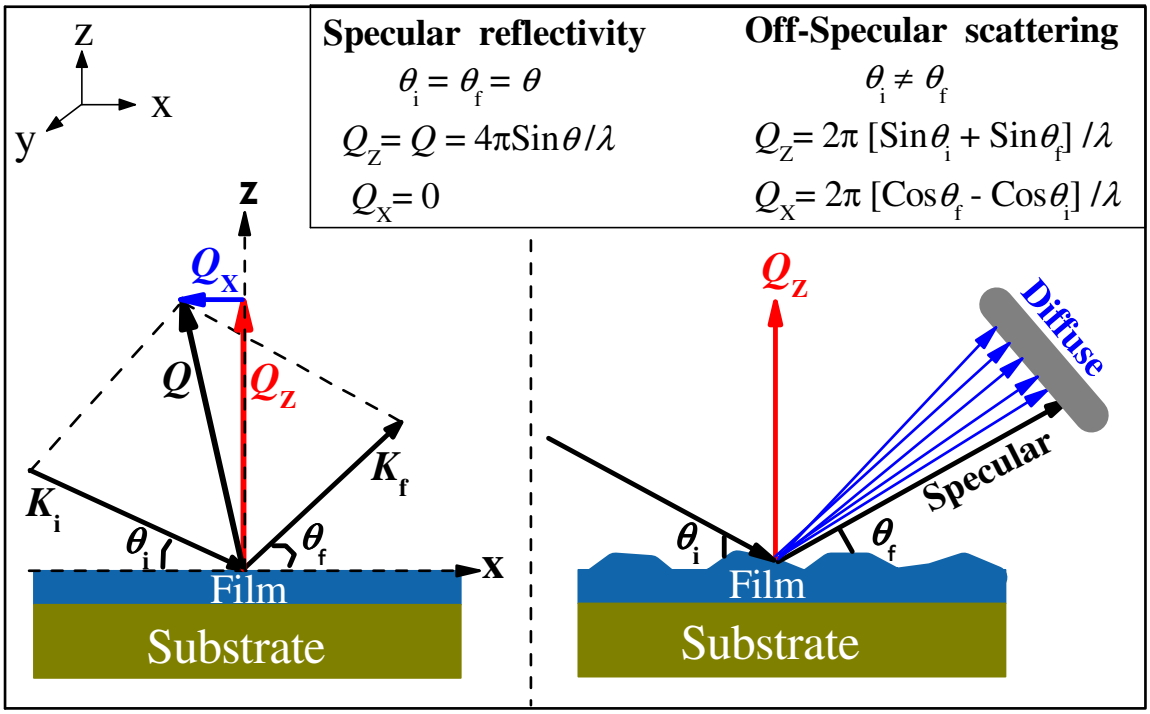

Figure 1: Geometry of specular neutron reflectivity and off-specular (diffuse) neutron scattering.

Neutrons, in the quantum mechanical approach, can be treated as a wave with a characteristic wavelength, λ, defined by the de Broglie relation:

$$\lambda = \frac{h}{m_n v} \qquad (1)$$

where *h,* $m_n$and *v,* are Planck's constant, the neutron mass and speed, respectively. The propagation of neutrons in any medium can be represented by the Schrödinger equation for the neutron wave function Ψ(r) in the medium, which is analogous to the wave equation for light
and leads to neutrons showing characteristic optical behaviour such as total reflection and refraction [32, 33]. The Schrödinger equation for the propagation of neutron beam in a medium can be written as:

$$-\frac{\hbar^2}{2m_n}\nabla^2\psi(\vec{r}) + V(\vec{r})\psi(\vec{r}) = E_k\psi(\vec{r}) \qquad (2)$$

where $\hbar$ is Planck's constant divided by 2π, *V* is the potential seen by the neutron, m_n is the mass of the neutron, $\vec{r}$is the position vector of the neutron with wave function ψ($\vec{r}$) and E_k (=$\frac{\hbar^2 k^2}{2m_n}$, where, *k*=2π/λ, is the wave vector of the neutron) its energy. In small angle limits, in which NR is measured and far from satisfying the Bragg condition of the crystalline structure, *V* represents a constant potential (as depicted in Fig. 2), the net effect of the interactions between the neutron and the stutterers in the medium through which it moves and is simply related to the coherent scattering length by the relation [34]:

$$V = \frac{2\pi\hbar^2}{m_n}\rho \qquad (3)$$

where ρ is the NSLD of the medium and it is defined as $\rho = \sum_i N_i b_i$, with N_i and b_i are the number of nuclei per unit volume and scattering length of nucleus '*i*', respectively. The scattering length *b*, change not only from one atomic species to another but also for the different isotopes of the same species because the interaction of a neutron with a nucleus depends not only on the atomic number of the nucleus but also on the total spin state of the nucleus-neutron system. In general, the value of *b* is a complex quantity and the imaginary part of *b* (=$\sqrt{\sigma_a/4\pi}$, where σ_a is absorption cross section for thermal neutrons) accounts for the absorption of the neutron in the medium. The absorption cross-section for neutrons is negligible for most of the elements, except for some elements e.g. Gd, Sm, B and Cd. Most of the elements (materials) in the periodic table have a positive *b,* which represents a positive potential for neutrons and thus has less kinetic energy. Neutrons seeing positive potential in the medium thus have a longer wavelength (opposite to light where the wavelength shortens) in the medium.

Consider a two-medium system, as depicted in Fig. 2 (a), with *k* and k_1, which are the wave vectors of incident neutrons in these mediums. In the non-relativistic limit, the energy of the neutron in the medium is given by:

$$E_1 = \frac{\hbar^2 K_1^2}{2m}; E_2 = E_n - V = \frac{\hbar^2 K^2}{2m} - V \qquad (4)$$

The wave vector of the incident neutron *k* changes to $k_1$under influence of the nuclear potential. This allows us to correlate the refractive index of the medium, *n*, to the NSLD (ρ) of the medium as given below

$$n^2 = \frac{k_1^2}{k^2} = 1 - \frac{4\pi\rho}{K^2} = 1 - \frac{\lambda^2}{\pi}\rho \qquad (5)$$

For most of the materials, the refractive index for neutrons is marginally less than unity and $\frac{\lambda^2\rho}{\pi}$ is typically in the range of 10^{-6} and reflection of neutrons takes place at grazing incidence as

stated earlier. Since the refractive index is less than unity, there will be a total external reflection for neutrons unlike optical rays (refractive index in the medium >1) where total internal reflection occurs. At the interface between two media, Snell's law applies i.e. for neutrons, $\cos\theta = n\cos\theta_1$. For the critical angle of incidence (θ_c), we have the condition $\theta_1 = 0$. Then we have $\cos\theta_c = n$ and using Eqn. (5) we get the expression for θ_c. i.e.,

$$\theta_c = \lambda\sqrt{\frac{\rho}{\pi}} \qquad (6)$$

For most of the materials, the critical angles are about a few arc minutes per Å wavelength. The corresponding momentum transfer vector for this angle of incidence is denoted Q_c ($= 4\pi\mathrm{Sin}(\theta_c)/\lambda$).

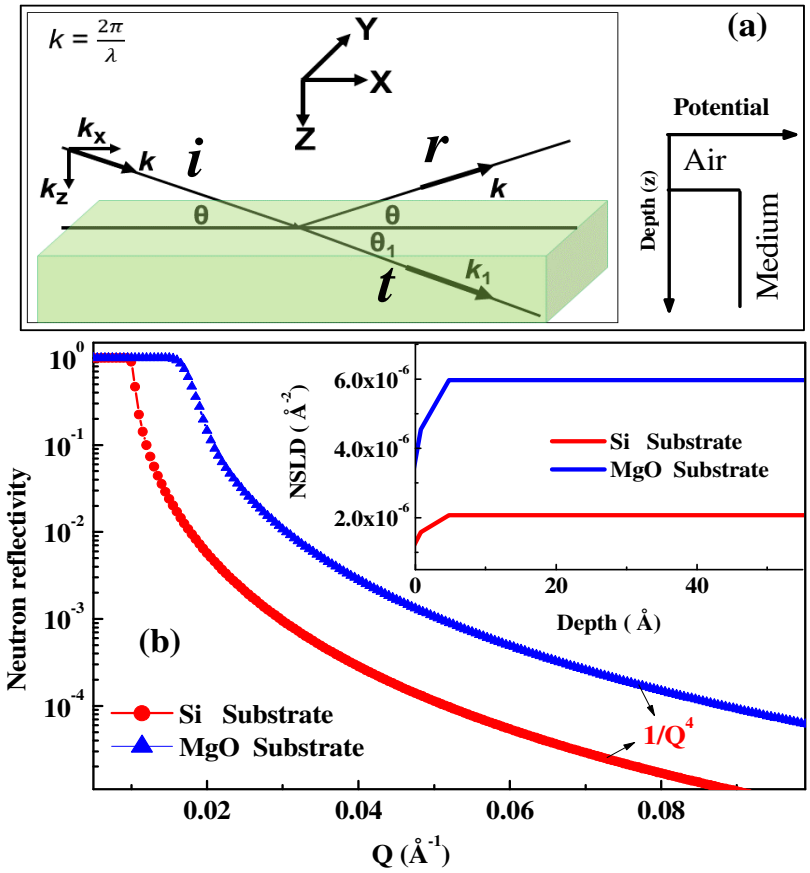

Figure 2: (a) Schematic of Neutron beam reflecting at sample surface with direction convention used. The k and k_1 are the incident (medium 1) and refracted (medium 2) wave vectors, with angles θ (angle of incident = angle of reflection for specular NR) in the incidence plane. On the right, the depth profile of the potential of the medium is represented.(b) Comparison of calculated specular NR patterns from two substrates, Si and MgO. The inset shows the NSLD profiles for these substrates.

If we consider a plane wave propagating in the z-x plane with the interface lying in the x-y plane and the stratification along the z direction (schematic is shown in Fig. 2 (a)), then the potential V depends only on one spatial variable z. The solution of Eqn. (2) may be written as:

$$\psi(z,x) = e^{iKx}\phi(z) \qquad (7)$$

Using Eqns. (6) and (2) one gets a second-order differential equation for ϕ:

$$\frac{d^2\phi}{dz^2} + q^2\phi = 0; q^2 = \frac{2m_n}{\hbar^2}[E_k - V] - K^2 \quad (8)$$

where q and K are z and x components of the wave vector k respectively. Considering the unit incoming neutron (i = 1), the reflection amplitude (r) and the transmission amplitude (t) are defined in terms of the limiting forms of the solution of Eqn. (8):

$$e^{iq_1 z} + re^{-iq_1 z} \leftarrow \phi(z) \rightarrow te^{iq_2 z} \qquad (9)$$

where q_1 and q_2 are defined in Eqn. (9) for two mediums (normal components of the wave vector in a vacuum and the medium, respectively), says, 1 and 2, which consist of an interface. A typical two-medium system with an incident neutron beam ($\boldsymbol{i}$ = 1), reflected beam ($\boldsymbol{r}$) and transmitted beam ($\boldsymbol{t}$), is represented in Fig. 2(a).

The intensity of the reflected specular signal from an ideally flat surface can be calculated by considering proper boundary conditions for neutron wave function Ψ(z) and its derivative at the interface. The result is known as Fresnel relationships, which give the amplitude of specular reflection and the transmission coefficient of the beam. If one considers an ideally flat surface with a sharp boundary, then the reflection/refraction, at an interface, can be represented by Fig. 2(a). In this figure, the neutron beam impinges the surface from the vacuum at a glancing angle θ, and the refracted beam propagates at an angle θ_1. k is the wave vector of the incident neutron. Considering the continuity of wave function ϕ (the solution of Eqn. (8)) and $\frac{d\phi}{dz}$ at the interface (i.e. Eqn. (9)), we get :

$$1 + r = t\,; \quad q_1(1 - r) = q_2\, t \qquad (10)$$

Solving these two equations for r and t, we get the reflection amplitude and transmission amplitude at the interface [32]:

$$r = \frac{q_1 - q_2}{q_1 + q_2};\; t = \frac{2q_1}{q_1 + q_2} \qquad (11)$$

where the normal component of wavevector in two mediums are $q_1 = \frac{2\pi}{\lambda} sin\,\theta$ and $q_2 = \sqrt{q_1^2 - 4\pi\rho}$. The Fresnel reflectivity for an ideally flat surface, for a glancing angle θ, is, defined as

$$R_f = |r|^2 = \left|\frac{q_1 - q_2}{q_1 + q_2}\right|^2 = \left|\frac{sin\,\theta - \sqrt{n^2 - cos^2\,\theta}}{sin\,\theta + \sqrt{n^2 - cos^2\,\theta}}\right|^2 \qquad (12)$$

From Eqn. (12), when cos θ >n then r is a complex number and the Fresnel reflectivity is unity, i.e. for $\theta < \theta_c$(critical angle of incidence) there will be a total external reflection of neutrons. Above the critical angle when $\theta >> \theta_c$, the reflectivity drops off as θ^{-4} (or Q^{-4}, where $Q = 2q_1$) and Eqn. (12) reduces to $R_f \approx \frac{16\pi^2}{Q^4}\rho^2$. This rapid drop in intensity beyond the critical angle makes reflectivity experiment intensity limited at larger angles. Using the Eqn. (12) we have simulated the NR profile for Si and MgO substrates and it is shown in Fig. 2 (b). The inset of Fig 2(b) shows the NSLD depth profiles of these substrates. It is evident from Fig 2(b) that the reflectivity from the MgO substrate is higher as compared to the Si substrate, which is due to the larger NSLD value for MgO. Neutrons see a higher change in NSLD (contrast) at the air-substrate interface for the MgO substrate and thus are reflected neutrons strongly.

Till now we have seen the NR from a single interface (air-substrate interface) consisting of two mediums. Calculation of NR for a single film grown on a substrate or a multilayer film grown on a substrate can be adopted following a similar approach and applying the boundary conditions at each interface of the heterostructures. The schematic of the heterostructure consisting of a single layer on a substrate and a periodic multilayer is shown in Fig. 3 (a) and (b), respectively, along with the potential depth profiles. When neutrons impinge on the film surface from the side of air from a single-layer heterostructure (Fig. 3(a)),interference occurs by a phase difference, corresponding to film thickness (d), between the neutrons reflected at the air-film interface (surface) and the film-substrate interface. General techniques such as the optical matrix method [35] or Parratt formalism [36] are used extensively to generate reflectivity profiles from heterostructures. Figure 3 (c) compares the specular NR profiles calculated for (i) a Si substrate, (ii) a thin film of deuterated polystyrene (dPS) with a thickness of 500 Å on a Si substrate, and (iii) a thin film of hydrogenated polystyrene (hPS) with thickness 500 Å on Si substrate. The profiles for the two polymer thin films exhibit regular oscillation due to interference of neutron beam reflected from air-film and film-substrate interfaces and these are called Kiessig fringes. The constant period of Kiessig oscillations corresponding to the film thickness (d) and the film thickness can be estimated by measuring the frequency of the fringes (ΔQ) using a relation $d = \frac{2\pi}{\Delta Q}$. The corresponding NSLD profiles for three different cases are shown in the inset of Fig. 3 (c).

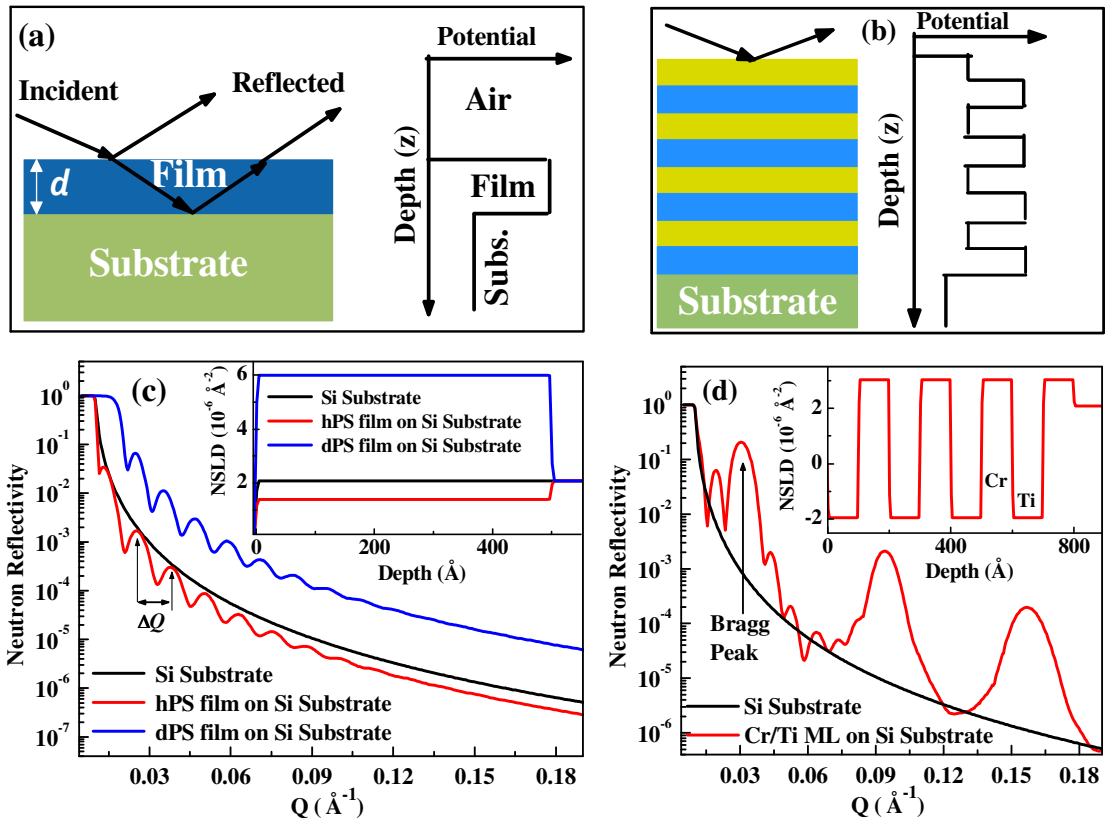

Figure 3: Schematic of neutron reflectivity and depth-dependent potential from (a) a single film and (b) a multilayer grown on a substrate. (c) comparison of calculated NR profiles from a Si substrate and a single film of the hPS (hydrogenated polystyrene) and the dPS (deuterated polystyrene) of similar thickness grown on a Si substrate. The inset shows the NSLD profiles. (d) comparison of calculated NR profiles for Si substrate and a multilayer of Cr/Ti (4 bilayers of Cr (~ 100 Å) and Ti (100 Å)) grown on Si substrate. The inset shows the NSLD depth profile of the multilayer.

It is noted that the neutron reflectivity for the dPS film is stronger than the hPS film, which is due to larger contrast (large change in NSLD at film-substrate and air-film interfaces) for the dPS

film. A larger NR signal can help to collect the data for a larger Q range and this helps to estimate the parameters from the NR technique with a higher confidence limit. This example also suggests the importance of the deuteration of biological thin films for neutron reflectivity or in general neutron scattering techniques. Figure 3 (d) shows the NR pattern generated using Parratt's formalism [36] for a Cr/Ti multilayer of 4 bilayers with a bilayer period of 200 Å (thickness of 100 Å for each Co and Cu layers, grown on Si substrate). The inset of Fig. 3 (d) depicts the NSLD profile of the multilayer representing periodic NSLD variation in 4 bilayers. Thus using NR we can get a detailed layer structure of the designed multilayer.

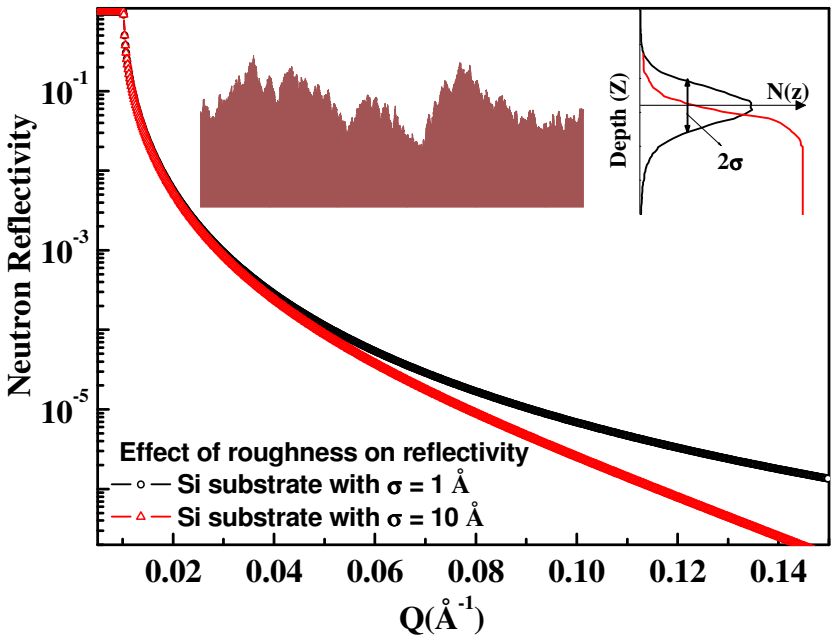

Figure 4: Effect of roughness on specular reflectivity from Si substrate with σ = 0 Å (solid line) and σ = 10 Å (dashed line). Inset (a) shows an image of a rough interface with a Gaussian profile of height. The standard deviation of the Gaussian function represents the root mean square roughness σ.

Above, I have discussed the reflection from heterostructures with flat interfaces. However, there is a large interest in what happens between materials at an interface. An interface may be rough with peaks and troughs over a large range of length scales with a fractal-like structure. For magnetic heterostructure, there may also have magnetic roughness if the magnetization does not sharply change at an interface. A boundary may be smooth but with one material diffused into the other. The other kind of inhomogeneity, which arises at the interface, is the mixing of two materials due to inter-diffusion. It is very important to incorporate the roughness, i.e., the random character of the interface, into the reflectivity calculation. It turns out that in both the rough and inter-diffusion cases the specular reflectivity is reduced by a factor very much like theDebye-Waller factor reduces scattered intensity from a crystal[37]. The inset of Fig 4 shows a typical rough interface with the profile of the random height distribution, which is a Gaussian. The standard deviation of the Gaussian function represents the root mean square roughness, σ. The reflectance for a Gaussian rough surface is modified as[4, 7, 37]:

$$r(Q) = r_F e^{-2Q^2\sigma^2} \qquad (13)$$

Where, r_F is Fresnel reflectance of the ideal surface given in Eqn. (12). Figure 4 shows the calculated NR profiles for Si substrates with a roughness of 1 Å (black open circles with line) and

10 Å (red open triangle with line). It is evident from Fig. 4 that the NR from a rough interface deviates from the ideal reflectivity for a smooth surface as a function of *Q*.

2.2 Polarized Neutron Reflectometry

Over the last 30 years, polarized neutron reflectometry (PNR) has contributed largely to investigating the interface magnetism in magnetic thin film heterostructures and magnetic multilayers. It is especially useful for functional materials and fundamentals of nanomagnetism, including exchange bias, multiferroic heterostructures, correlated electron systems, superconductors, magnetic nanoparticles and spin textures like skyrmions. Neutrons have a spin$\vec{\sigma}$, related to the magnetic moment $\vec{\mu}_n$ of the neutron by the vector operator:$\vec{\mu}_n = \mu_n\vec{\sigma}$, With μ_n = -1.913 β_N andβ_N the nuclear magnetron ($=e\hbar/2m_nc$). For a medium in which the scattering centres have magnetic moments, neutrons, because of their inherent magnetic moment, will experience an additional potential energy in a magnetic field *B*, other than the nuclear potential, given by:

$$V_{mag}(r) = -\vec{\mu}.\vec{B} \qquad (14)$$

where $\vec{\mu}$ is the magnetic moment of the neutron and $\vec{B}$ is the magnetic field. It is clear that depending on the relative orientation of the neutron magnetic moment and the local field the magnetic potential (whether parallel or anti-parallel) can have a positive or negative value with respect to the nuclear potential. One may now write the total potential for the magnetic film as a summation of the nuclear and the magnetic parts as given below

$$V_{tot}(r) = \frac{2\pi\hbar^2}{m}(\rho_n \pm \rho_m) \qquad (15)$$

where (+) and (-) signs correspond to the spin-up and spin-down neutrons with respect to sample magnetization. Using this potential one can solve the Schrödinger equation given in Eqn. (2) for calculation of the reflectivity from the magnetic medium in a similar way as given for unpolarized NR in the previous section. Now using Eqn. (5) and (6) the refractive index and critical angle for a neutron in a magnetic medium can be written as:

$$n = 1 - \frac{\lambda^2}{2\pi}(\rho_n \pm \rho_m); \qquad \theta_c = \lambda\sqrt{\frac{(\rho_n \pm \rho_m)}{\pi}} \qquad (16)$$

For calculating the PNR profile from a magnetic multilayer, there are formalism developed by C.F. Majkrazk[5] and G. P. Felcher[31], which describes the specific case of the neutron polarization axis being parallel to the sample surface. Parratt [36] formalism and the matrix formalism given by Blundell and Bland [35]are also used to generate the theoretical PNR profile and both give identical profiles.

Figure5 shows a simulated polarized neutron reflectivity plot, of a Fe/Cr multilayer with 10 bilayers of Fe (thickness 60 Å) and Cr (50 Å) grown on Si substrate, as a function of wave vector transfer *Q*. For simulating the PNR profile, we have used the bulk magnetic moment (2.20μ_B) for Fe atom. The reflectivity pattern is generated using Parratt formalism [36]. The difference in the reflectivity pattern of the sample for the spin-up and spin-down neutrons is due to the difference in the step potential due to the magnetic part of the Fe layers for the spin-up and spins-down neutrons. The change in critical angle (Eqn. 16) for the two spins is also evident in Fig. 5.

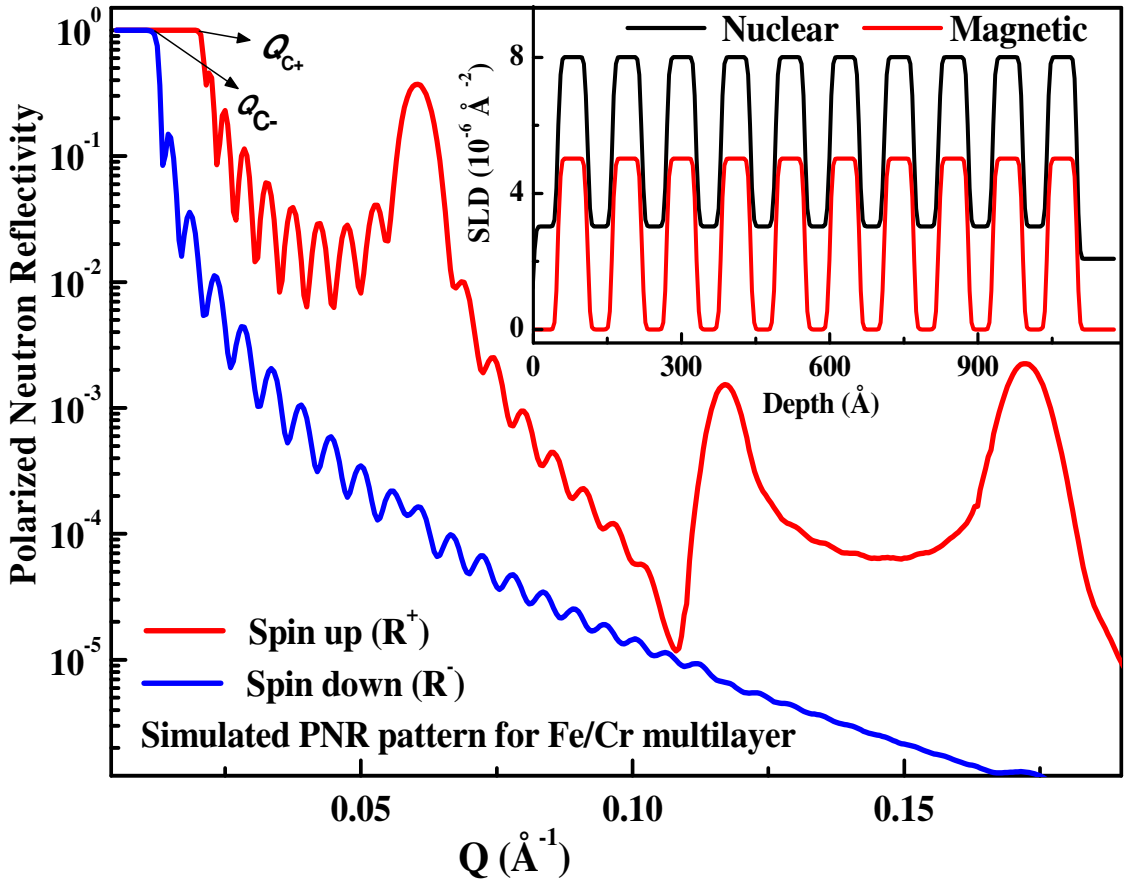

Fig. 5: Calculated polarized neutron reflectivity pattern for Fe/Cr multilayer.

In addition, if one needs to determine the in-plane magnetization vector(both magnitude and direction) and the nature of magnetic coupling in more complex magnetic multilayers the analysis of the polarization state of the reflected neutron beam is required. In this case, one obtains four reflectivity profiles with non-spin flip (NSF) (R^{++}, R^{--}) and spin-flip (R^{+-}, R^{-+}) modes. In the first approximation, the non-spin flip (NSF) components determine the component of the magnetic moment parallel to the quantization axis (or parallel to neutron spin) and the spin-flip (SF) components determine the perpendicular component. PNR in polarization analysis mode has provided valuable information on the nature of magnetic coupling in GMR multilayers and helped in understanding the nature of spin-dependent electron transport in these materials.

3 Neutron Reflectometer Instrumentation and Data Analysis

A number of neutron reflectometers are currently working at both types of neutron sources worldwide: a reactor and a spallation neutron source. In fact, every neutron facility in the world holds at least one reflectometer for carrying out structural studies on interfaces and thin films for a variety of materials. The conventional reflectometer, without a polarization option (for unpolarized NR measurements), has a relatively simple configuration, in which a pair of incident slits, a sample stage and a neutron detector are arranged in a sequence from neutron sources. The slit blades are made of a neutron-absorbing material such as cadmium, and the two incidents are separated from each other by approximately a few meters to produce a well-collimated beam falling on the sample table. The sample and the detector are mounted on goniometers or translation tables to make them arrange precisely at the proper angular position relative to the incident beam. While in the case of PNR measurements two additional components, polarizer and spin flipper are required to be added. Figure 6 shows the schematic of a PNR instrument. Depending on the type of neutron source (a

monochromatic neutron beam usually from a reactor source or neutrons with a spread of wavelength usually from a spallation source) one can cover the reflectivity as a function of momentum transfer by changing the angle of incidence (reactor)/wavelength (spallation).

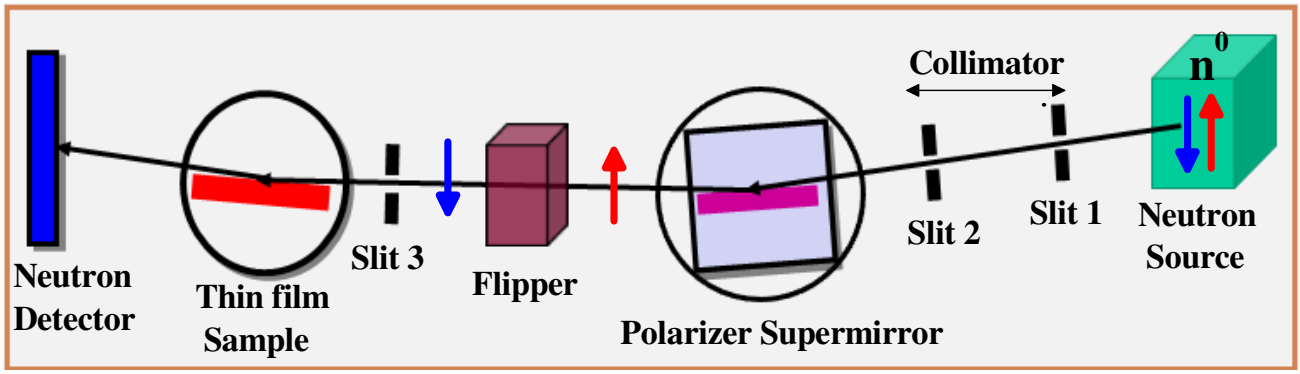

Figure 6: Schematic of a typical PNR instrument, which measures the spin-dependent reflectivity (R^+, spin-up and R^-, spin-down).

There are many neutron reflectometers available around the world in major neutron sources, which are being used for studying the interfaces. The full compilation of neutron reflectometers and the related data analysis program is available online [38]. A PNR instrument is available at the DHRUVA reactor, BARC, India[39, 40], which is designed for vertical sample geometry for PNR measurements without a polarization analysis option and is thus being used to investigate the magnetization depth profiles of thin films[4]. This instrument has been positioned on thermal neutron guide G2 in the Guide Tube Laboratory (GT Lab) of Dhruva Reactor, which uses a monochromatic neutron beam with a wavelength of λ ~ 2.9 Å and a linear position-sensitive detector (PSD), where only a sample is rotated to cover the desired Q range. Linear PSD also helps to collect both specular and off-specular reflectivity simultaneously at each angle of incidence[4, 39, 40].

In reflectometry, the reflected intensity is measured as a function of momentum transfer Q. The measured reflectivity is a convolution of reflectivity with the resolution of the instrument. To compare the measured data with the calculated data, first, we have to correct it for the instrumental resolution. This can be done either by, deconvoluting the measured data for experimental resolution or convoluting the theoretical profile with an experimental resolution before comparing it with experimental data. The instrumental resolution in small angle approximation is given by:

$$\frac{dQ}{Q} = \sqrt{\left(\frac{d\theta}{\theta}\right)^2 + \left(\frac{d\lambda}{\lambda}\right)^2} \qquad (17)$$

The typical wavelength resolution $(\frac{d\lambda}{\lambda})$ for a single crystal monochromator-based reflectometer is ~ 1 to 1.5%. The major contribution comes from the divergence of the neutron beam which can be varied by selecting different widths of slits and the typical Q resolution $(\frac{dQ}{Q})$ of a reflectometer can be chosen around 1 to 3%. Usually, the reflectivity profile is measured for a constant value of $\frac{dQ}{Q}$ in the whole range of Q, which is done by choosing the appropriate combination of slits for various Q ranges.

4 Interface Structures in Soft Matter Using Unpolarized Neutron Reflectivity

During the last decades, the use of unpolarized NR techniques in biological sciences has grown enormously[41]. This technique was introduced in the 1980s for the study of surfactant thin films and since then the improvements in neutron instrumentation, sample environment and modelling approaches have made this technique a critical tool for investigations of systems of increasing complexity. NR has emerged as a versatile tool for examining structural complexity at interfaces. This technique has been used to reveal the depth-dependent structure of biological samples including cell membranes, protein film, and a combination of protein and cell membranes, which is the most investigated class of the bio-relevant systems using NR. To understand the molecular processes involved in diseases and the development of new drugs, the interactions of proteins/peptides within and at the surface of cell membranes are essential [42].As mentioned earlier, NR has been widely utilized for the investigation of depth profiling of structural properties on a variety of material interfaces and thin films for soft matters and biology: a polymer thin film, a Langmuir–Blodgett (LB) film, a Gibbs or a Langmuir monolayer of amphiphilic molecules such as surfactants, lipids, block copolymers, and proteins on the water surface, a polymer brush chemically or physically adsorbed on a solid substrate, and so on. Recently, NR in combination with X-ray reflectivity (XRR) was also being used to study the emerging field of liquid metals, organic liquids, liquid crystals, and ionic liquids for the understanding of the fundamental physics of liquid surfaces. Here, we will briefly describe the results on two systems, already published in litrature, highlighting the capability of NR.

4.1 Biological membranes

Bio-membranes are chemically diverse and complex molecular assemblies at the basis of life [43]. Cell membranes are active barriers for performing different and fundamental processes such as regulating cell growth, controlling the selective exchange of substances between inner and outer cellular environments and recognizing external stimuli [44]. Because of their nanometric thickness, they are perfect systems to be studied using NR [45]. Lipid bilayers are the basic building units of biological membranes and several biological processes involve revolutions between such bilayer structures, which are studied using unpolarized NR measurements. Phospholipid bilayers have been intensely used as model systems for studying the structure and interactions of biological membranes[46], which exhibit a main phase transition from a gel phase to a liquid crystalline phase [47].In case of gel phase, lipid chains are rigid and well ordered, while in the liquid crystalline phase the chains are disordered and fluid like and such phase transition can be achieved by change the temperature of the system [47]. Such a structure phase transition in these biological model system can be studied using NR technique.

Figure 7 (a) shows a schematic of model system consisting of two bilayers (gel phase), one adsorbed on a flat surface of the Si substrate and a second floating at 20 to 30 Å above the first in bulk heavy water (D_2O). We have also shown the NSLD depth profile, which represents the variation of NSLD at different depth as per the structure of model lipid bilayer system in D_2O medium, by blue line in Fig. 7 (a).In addition, we have also considered two more situations as shown in Fig. 7(b) and (c), where the bilayer lipid systems, shown in Fig. 7(a), show distortion from the gel phase. Figure 7 (b) shows the fluid phase where the lipid bilayer shows fluctuation in the position making the system with more roughness at different interfaces. The corresponding NSLD depth profile (blue solid line) is also depicted in Fig. 7 (b). Figure 7 (c) shows some intermediate phase where the separation between two bilayer also increases in addition to fluctuation in the top bilayer lipid. The corresponding NSLD profile is depicted in Fig. 7 (c). We have calculated the unpolarized NR profiles for these three situation and shown in Fig. 7(d), (e) and (f), respectively. IT is evident from Fig. 7 that the depth dependent fluctuation in this bio-interface system can be revealed using NR successfully. The similar depth dependent structure was also measured experimentally using NR for a hydrogenated di-stearyl phosphatidyl choline (DSPC)in D_2O as a function of temperature [47].

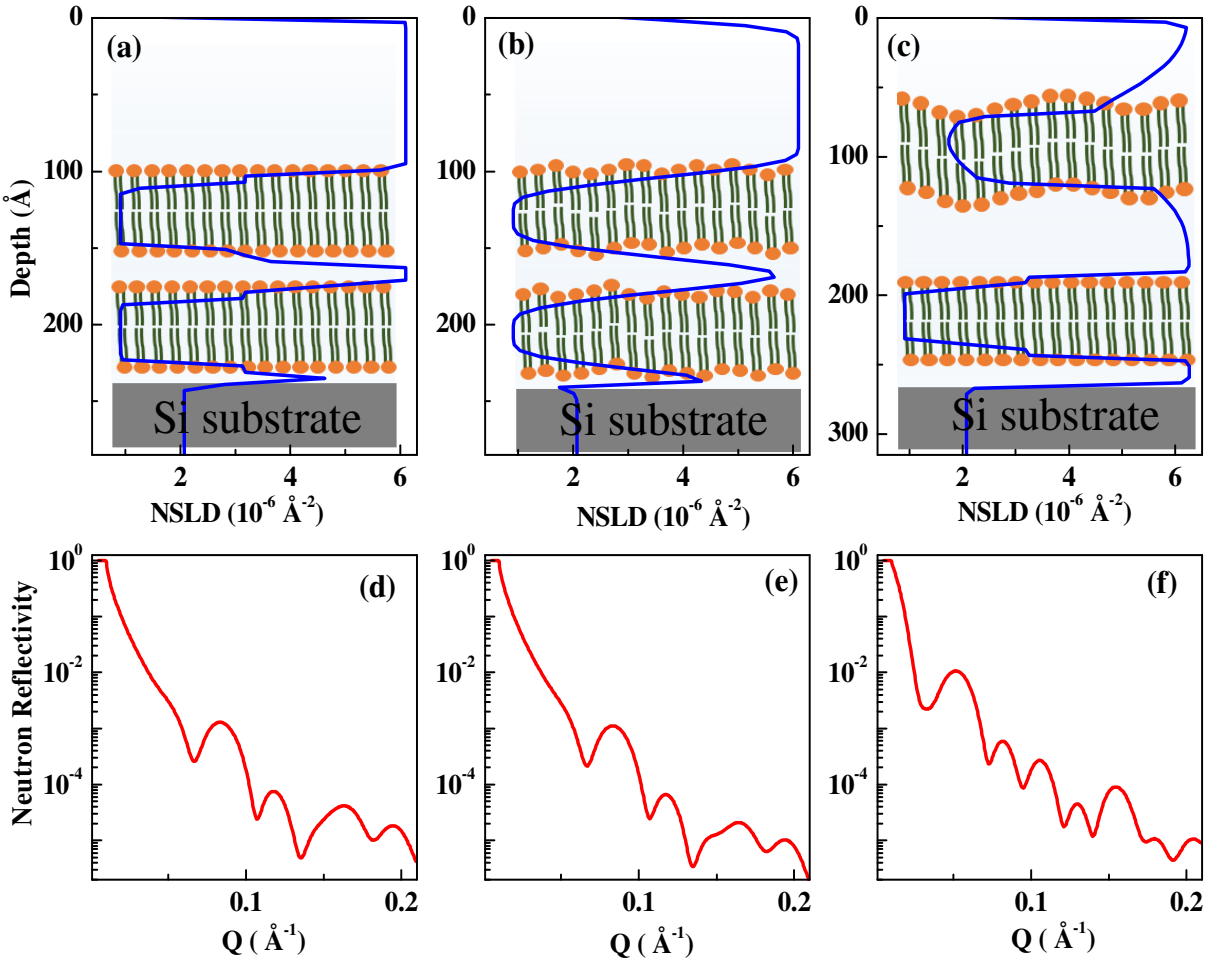

Figure 7: (a) Schematic model system of a biological membrane consisting of two lipid bilayers (gel phase), one adsorbed on a flat surface of the Si substrate and a second floating at 20 to 30 Å above the first in bulk heavy water (D_2O). The schematic of the two bilayer system with disorder is represented in (b) and (c). The Blue line shows the corresponding NSLD depth profiles. (d) to (f):The calculated NR patterns for three different models (shown in (a) to (c)).

4.2 Biomolecules at the interfaces and its interaction with membrane

Adsoption of biomolecules at interfaces, especially protein, provide an excellent opportunity and very active research area for which NR can contribute significantly. Though there are many techniques (e.g. ellipsometry, quartz crystal microbalance, atomic force microscopy etc.) which can be used to estimate the amount of absorebed materials and related kinetics. NR is a characterization tool which provide detail organization of protein molecules at interfaces and it can uniquely study the exact location of protein molecules from the interfaces as well as formation of multilayers due to adsoption. Using NR, Mazzer*et al.*[48]studied the adsoption of immunoglobulin G (IgG) at various solid-liquid interfaces and NSLD depth profiles suggested the resistance of protein adsorption at the surfaces. Interaction of molecules with lipids permeate the daily life of human beings and NR allows to study these fundamental interaction not accessible by means of other techniques. The excellent use of NR in combination with other techniques for studying the protein-membrane interactions is given by Martel et al.[49], where they have investigated the amyloidogenicity and cytotoxic mechanisms of an amyloid polypeptide in type 2 Diabetes Mellitus. Using NR they could quantify and localize the structural changes induced in a solid supported bilayer (membrane) by modeling the NR data with different depth profiling of NSLD values.

5 Emerging Phenomena at Interfaces of Magnetic Heterostructures Using Polarized Neutron Reflectivity

5.1 Non-magnetic Co film at Interfaces

3*d* transition metals e.g. Fe, Co and Ni show interesting magnetic properties both in their bulk and thin film form. Co in bulk shows a hexagonal closed pack (*hcp*) structure. However, the theory predicted that a high-density face-centred-cubic (*fcc*) phase of cobalt can be nonmagnetic [17, 50]. There was no experimental study in the literature for Co showing highly dense nonmagnetic properties. We investigated the depth-dependent structure and magnetic properties of a number of Co thin films (thickness of ~ 200-300 Å) deposited with different buffer layers on Si [111] single crystal substrate using PNR as a primary technique[17, 50]. PNR experiments in combination with other measurements confirmed the formation of a high-density Co layer at both interfaces (film-air or surface and substrate-film) of the film when Co was grown directly on Si layers. The PNR experiments were carried out at Dhruva. PNR results also suggested that the high-density interfacial Co layer is nonmagnetic. Figure8 (a) and (b) show PNR data (symbols) as a function of the ratio of momentum transfer to the critical value of momentum transfer (Q/Q_c) along with fits (solid lines) from the Co film at room temperature (RT) grown on Si and SiO_2/Si substrates, respectively. Figure8 (c) and (d) show the NSLD and MSLD depth profile of these heterostructures, which best fitted the PNR data at RT. The NSLD depth profile of the film obtained from the Co film grown on Si substrate (Fig. 8 (a)) indicated the presence of high-density (HD) Co layers at both interfaces [Fig. 8 (c)] i.e., film-air and film-substrate interfaces. Most interestingly, the HD Co layers at the interfaces were non-magnetic as can be seen in the MSLD (Fig. 8 (c)) depth profile obtained from PNR. Remarkably, when Co film was grown on SiO_2/Si substrate [Fig. 8 (b) and (d)] we did not obtain the HD Co layer formation at the interfaces.

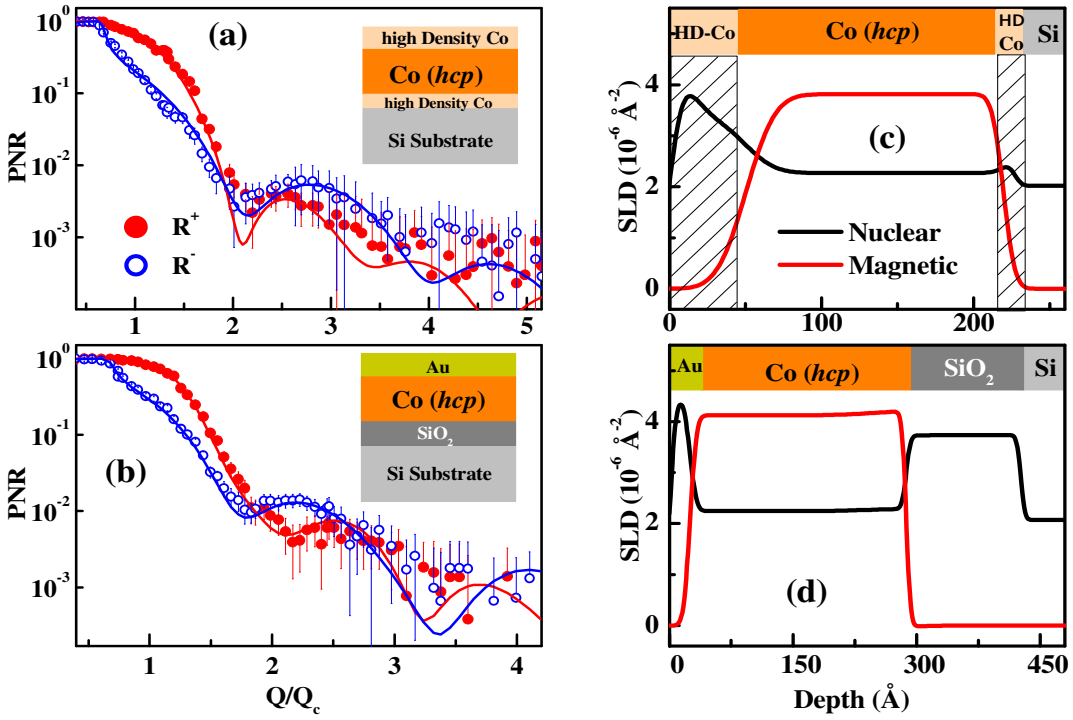

Figure 8: PNR data (symbol) and corresponding fits (solid lines) from Co films grown on (a) Si and (b) SiO_2/Si substrates. Insets (a) and (b) show a schematic of the corresponding film obtained from the PNR results. The NSLD and MSLD depth profiles obtained PNR results for Co films

grown on (c) Si and (d) SiO_2/Si substrates. Co film grown on Si substrate suggested the formation of high density (HD) Co layer at both the interfaces which are non-magnetic.

It was also confirmed from high-resolution cross-sectional transmission electron microscopy that these high-density layers were of *fcc* structure unlike bulk Co, which has an *hcp* structure. Thus, it was conjectured that the migration of Co atoms along grain boundaries during deposition might have caused high pressure during the growth and given rise to such a phase at the interfaces, as the *fcc* phase can exist at high pressure. This unique result vindicated the strength of PNR in detecting such ultra-thin layers and their magnetism. These results demonstrate the fact that PNR plays an important role in obtaining such properties with excellent spatial resolution in sub-nanometer length scales.

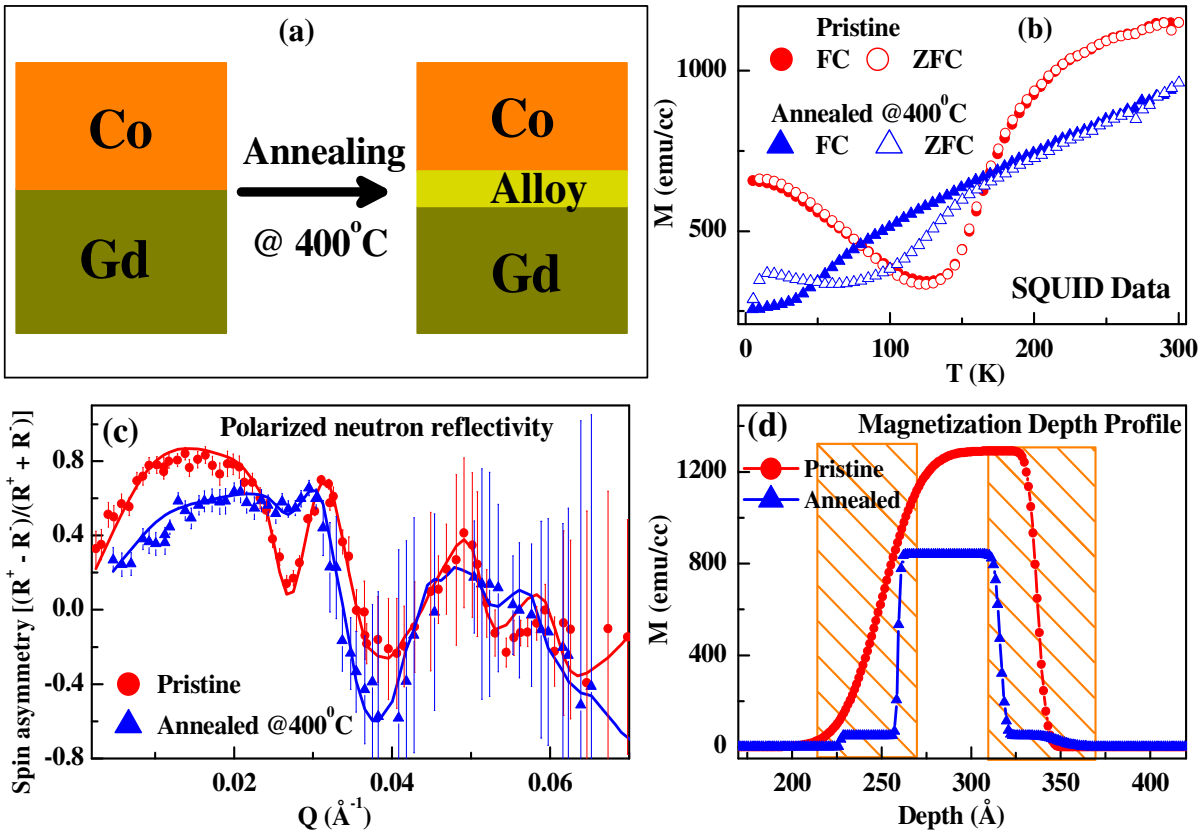

Figure 9:(a) Schematic of a bilayer of Gd/Co multilayer before and after annealing the multilayer. (b) $M(T)$ data in FC and ZFC mode from as-deposited (pristine) Co/Gd multilayer and multilayer annealed at 400 °C.(c) PNR data and corresponding fit from multilayer.(d) Magnetization depth profiles at two interfaces were obtained from PNR.

5.2 Interface-Induced Magnetization in Co/Gd Multilayers

Rare earth (RE)–transition metal (TM) heterostructures, viz Gd-Fe, Gd-Co etc., are known to exhibit several magnetic structures at different temperatures and magnetic fields due to the strong antiferromagnetic (AF) interaction at the interfaces. Co and Gd show long-range magnetic order with a Curie temperature of ~ 1400 K and 293 K, respectively. Interface structure and morphology tend to play important roles in the magnetic properties of such systems. Using the polarized neutron reflectometer at Dhruva, we have investigated the structure and magnetic properties of Gd/Co multilayers at a nanometer length scale with an emphasis on the interface-induced phenomena. Interfacial dependence magnetic properties in this system were achieved either by depositing the multilayer using different growth parameters or annealing the multilayer samples[51, 52]. We have studied Gd/Co multilayer with a repeat of 10 bilayers of the Gd (thickness = 135 Å) and Co(thickness = 80 Å). Figure 9(a) shows the schematic of a bilayer of Gd/Co before (as-deposited

state, pristine) and after annealing the multilayer at a temperature of 400 ^{o}C for 0.5 hr. A comparison of macroscopic magnetization [$M(T)$], measured using SQUID magnetometer before and after annealing under field-cooled, FC, (at an applied field of 500 Oe) and zero fields cooled (ZFC) are shown in Fig. 9 (b), suggesting temperature dependent modulation in the magnetization. Figure 9 (c) shows the PNR data (symbols) and corresponding fit (continuous lines) in the representation of spin asymmetry, defined as the ratio of the difference and sum of spin-dependent reflectivity $[(R^+ - R^-)/(R^+ + R^-)]$.Figure 9 (d) shows the magnetization depth profiles across the interfaces of a Gd/Co bilayer in the pristine and annealed states. PNR data suggested the formation of an alloy layer at the interface with reduced magnetization at both interfaces (Co/Gd and Gd/Co). This change in the interfacial structure and magnetic properties of the multilayer may be contributing to the modification in the exchange interaction resulting in a change in the macroscopic properties of the multilayer. Therefore, the PNR results as a function of interface structure and morphology in the Gd/Co multilayer systems [51, 52] offered valuable information to help us understand the mechanisms of interface-induced magnetization in RE/TM systems. These results also suggested that a more complicated model which takes into account interface roughness and morphology in RE/TM systems is required to study these systems micro-magnetically for possible future applications.

5.3 Proximity and Tunneling at interfaces in Superconductor and Ferromagnet Oxide Heterostructures

It is well-known that superconductors are perfect diamagnets that do not coexist with ferromagnets. This fact brings an interesting question to the fore: what happens if a superconductor (SC) and a ferromagnet (FM) are brought closure to each other? Moreover, recently this problem has attracted a large number of theoretical and experimental studies on a phenomenon known as the *"proximity effect"* [21-23, 53, 54], which showed suppression of magnetism on the FM side with the formation of a magnetic depleted (MD) layer below superconducting transition temperature (T_{SC}). Using the inherent capability of PNR, we have observed modulation in the interfacial magnetization of the FM layer below $T_{SC,}$ even separating the FM layer from the SC layer by an insulator (I), which was described in terms of leakage of the spin-triplet Cooper pairs into the FM layer, leading to a modulation in the magnetism of the interfacial FM layer[21-24]. Here we describe the observation of suppression of the ferromagnetic order and the influence of ion irradiation and sequence of layer stacking on ferromagnetic order in $La_{2/3}Sr_{1/3}MnO_3$ (LSMO) layer separated from a $YBa_2Cu_3O_{7-\delta}$ (YBCO) layer by a thin oxide insulator $SrTiO_3$(STO). The hybrid heterostructures were grown on a single crystal MgO substrate by pulsed laser deposition technique [21].Combining structural and macroscopic magnetization measurements using XRD and SQUID, with PNR measurements we correlated the structural and magnetic properties across $T_{SC.}$ Figure 10 shows the comparison of different measurements on 3 hybrid heterostructures shown in the left column.

The top panel of Fig. 10 shows the schematic and different measurements for the MgO/YBCO/STO/LSMO heterostructure. The middle panel of Fig. 10 shows different measurements from the same heterostructure after ion irradiation with 120 MeV Ag^{15+} ions at a dose of 1×10^{12} ions/cm^2. While the bottom panel of Fig 10 shows the schematic and measurements from the MgO/LSMO/STO/YBCO heterostructure, where we have reversed the sequence of the layer. The XRD data from all three systems have shown crystalline structure for the YBCO layer with highly textured in the [00l] direction[22-24]. A comparison of SQUID data for the heterostructures suggested that heterostructure MgO/YBCO/STO/LSMO showed a T_{SC} of ~ 68 K (upper panel of Fig. 10), which reduces to 30 K (middle panel of Fig. 10) on ion irradiation and increases to 86 K (comparable to bulk value ~ 92 K for YBCO) on reversing the sequence of the layer growth. This change in $T_{SC}$is directly correlated to the atomic structure of the YBCO layer. It is evident from Fig. 10 that upon ion irradiation the Bragg peak shifts to a lower angle (middle panel), whereas changing the growth sequence shifted the Bragg peak to a higher angle (lower

panel), suggesting the expansion and compression of the lattice constant along *c* direction of YBCO layer on irradiation and sequence change, respectively. The PNR measurements were carried out on these heterostructures across $T_{SC,}$ which revealed the detailed magnetization depth profiles at different temperatures. The magnetization depth profiles at 10 K from these heterostructures are shown at the extreme left of each panel Fig. 10, suggesting the formation of the MD layer at the STO/LSMO interface. The interfacial LSMO layer in the magnetization depth profiles is highlighted as a shaded region. A thicker MD layer of thickness ~ 35 Å was observed for the MgO/YBCO/STO/LSMO heterostructure (upper panel), which reduces to (a) zero Å upon ion irradiation of the heterostructure (middle panel) and (ii) to a thickness of ~ 20 Å for heterostructure with reversed sequence (lower panel) below T_{SC}. The formation of the MD layer below T_{sc} in these heterostructures is attributed to the tunnelling of Cooper pairs across the insulator. This finding has demonstrated the need for PNR to understand the interplay of superconductivity and magnetism in such hybrid systems.

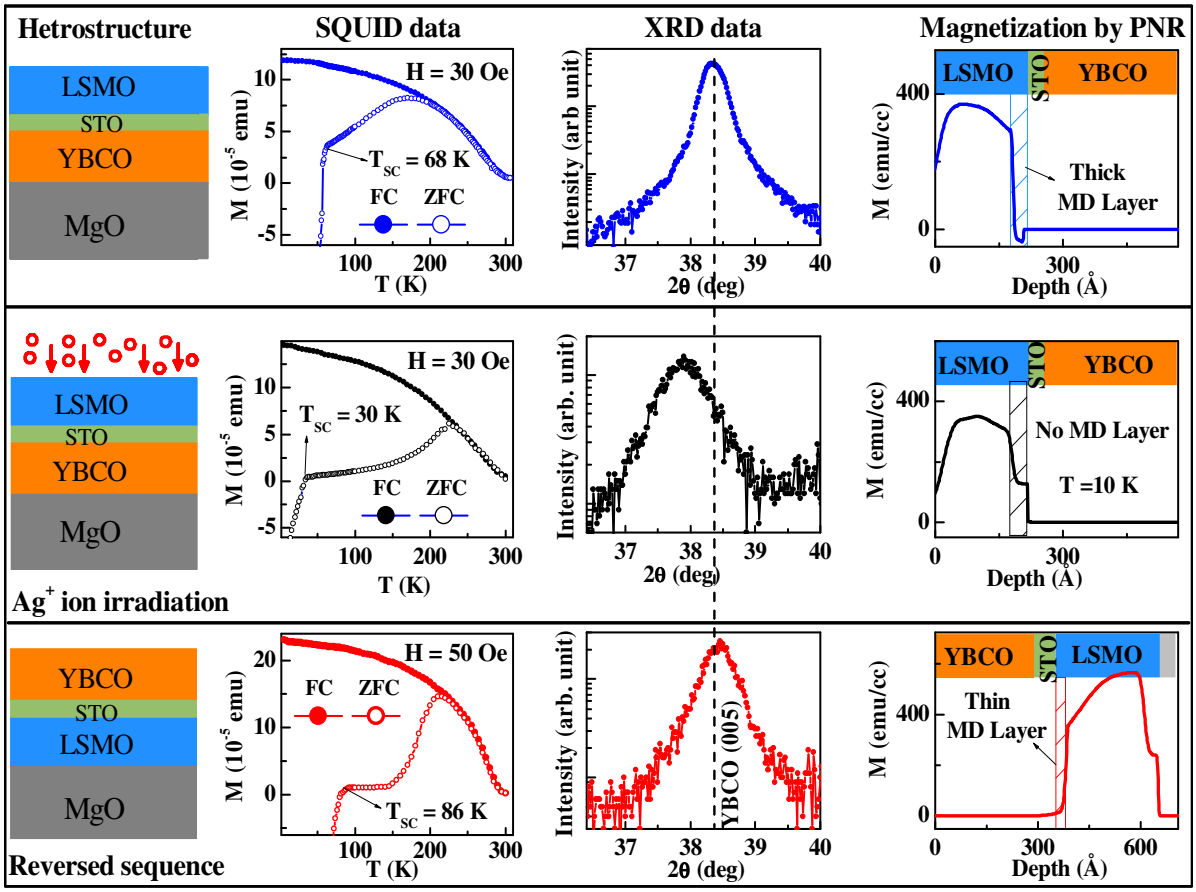

Figure 10: Comparison of XRD, SQUID data and magnetization depth profiles (PNR results) from trilayer heterostructures of YBCO-STO-LSMO grown on MgO substrates. (top panel) schematic of MgO/YBCO/STO/LSMO heterostructure with different measurements. (middle panel) ion irradiated MgO/YBCO/STO/LSMO heterostructure with different measurements. (lower panel) schematic of MgO/LSMO/STO/YBCO (reversed sequence) heterostructure with different measurements. The magnetization depth profiles extracted from PNR measurements for these heterostructures at 10 K are shown at the extreme right of each panel.

5.4 Induced Interface Magnetism at Ferromagnetic/Multiferroic Interface

The spin, charge and orbital reconstructions at interfaces in complex oxide heterostructures have driven several fascinating interfacial phenomena. Heterostructures involving oxide

ferromagnets such as $La_{0.7}Sr_{0.3}MnO_3$or $La_{0.67}Sr_{0.33}MnO_3$(LSMO) and oxide antiferromagnet such as$BiFeO_3$ (BFO) is the one which has been explored extensively [16, 55-58]. BFO is a single-phase multiferroic material which exhibits magnetoelectric coupling between ferroelectric, FE, (T_C= 1103 K) and antiferromagnetism, AFM, (T_N= 643 K) order parameters [59]. Theoretical calculations have suggested a weak FM for BFO (~0.03 μ_B) as a consequence of canting of the AFM structure due to the Dzyaloshinskii-Moriya interaction[60]. Experimentally, an enhanced magnetic moment (~ 0.75 μ_B) in the BFO layer in BFO/LSMO heterostructure was observed right at the interface, which was attributed to Fe-Mn hybridization and orbital reconstruction[55]. PNR measurements from BFO/LSMO heterostructures have also suggested an enhanced magnetization (~ 0.75 μ_B to 1.5 μ_B) for the Interfacial BFO layer of thickness ~6 to 8 unit cells and also suggested the presence of both types of magnetic coupling, FM (magnetic moment of interfacial BFO layer and LSMO are in same directions along the applied field) and AFM (moments are opposite, i.e. the magnetic moment of the interfacial BFO layer is opposite to applied field and LSMO layer) [16, 57, 58]. The different magneticcouplings in this system have also been confirmed by the first principal calculations and it was attributed to different surface terminations[16, 58].

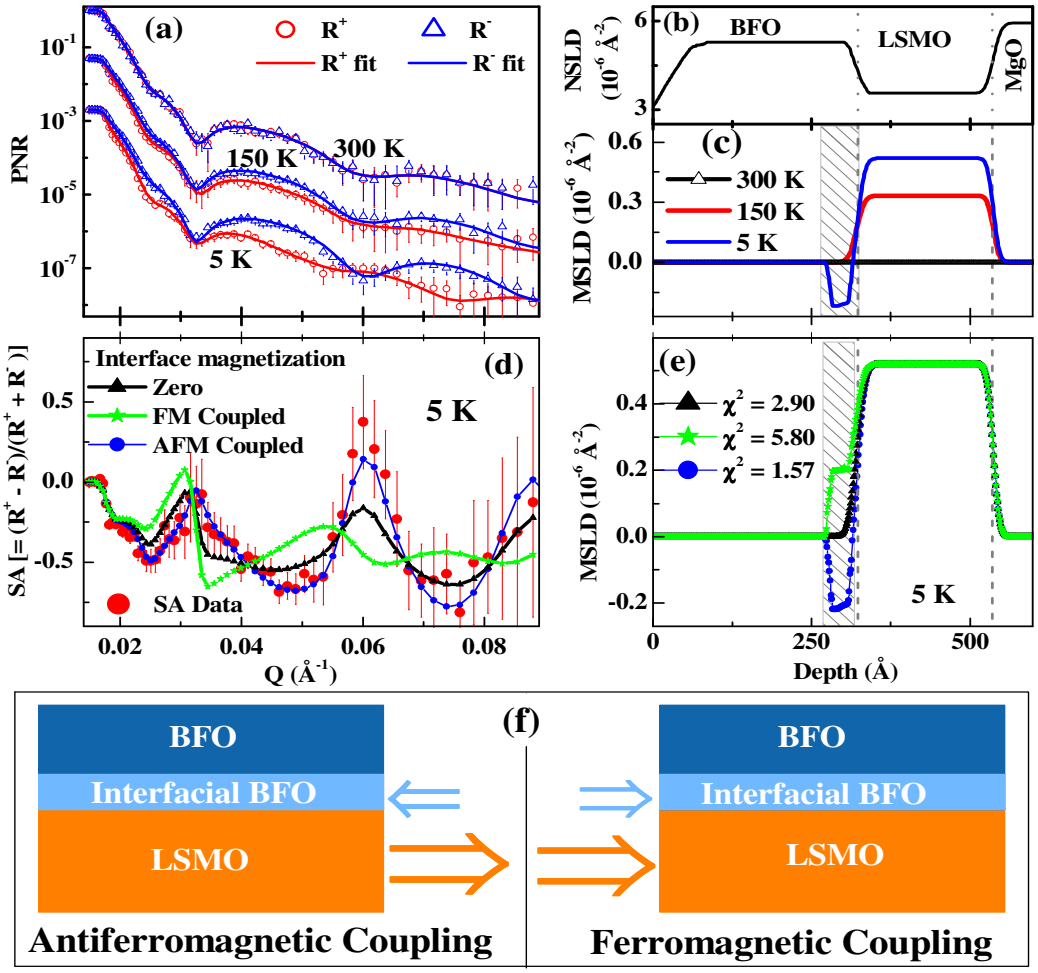

Figure 11: (a) PNR measurements at different temperatures from a MgO/LSMO/BFO heterostructure. The NSLD (b) and MSLD (c) depth profiles of the system were obtained from PNR at different temperatures. (d) Comparison of fits to spin asymmetry (SA) data (PNR data) considering different magnetization depth profiles as shown in (e). (f) different magnetic coupling between the LSMO layer and the interfacial BFO layer.

Figure 11 (a) shows the PNR measurements at different temperatures for the LSMO/BFO heterostructure grown on the MgO substrate. Spin-dependent (R^+ and R^-) PNR data (symbol) at 300

K did not show any difference (R^+ and $R^-$are the same) suggesting the system is nonmagnetic at this temperature and a detailed NSLD depth profile (Fig. 11 (b)) for the system was obtained from PNR data at 300 K. PNR measurements at low temperatures showed a splitting in R^+ and R^- data, suggesting FM behaviour of the system and detail MSLD depth profiles obtained at different temperatures are shown in Fig. 11 (c). PNR data at 5 K suggested that the interfacial BFO layer (thickness ~ 35 Å) is ferromagnetic with the magnetization aligned opposite to the applied field and magnetization of the LSMO layer (AFM coupling). To justify the magnetization depth profile obtained from PNR at 5K we have also assumed different magnetization profiles and a comparison of fit to PNR data and different magnetization profiles are shown in Fig. 11 (d) and (e), respectively. It is evident from Fig. 11 (d) and (e) that the magnetization depth profile assuming AFM coupling between the LSMO layer and the interfacial BFO layer best fitted the PNR data at 5 K. We have also studied different heterostructures of LSMO/BFO using PNR and observed both FM and AFM coupling as depicted in Fig. 11 (f).

5.5 Other Examples of Emerging Interfacial Magnetism using PNR

The existence of different magnetic orders at interfaces, which are different from their constituent bulk phase, have been reported, e.g., ferromagnetism at interfaces between two different AFM oxides [61-63] and between a paramagnetic metal and AFM insulator oxides [64, 65], a ferromagnetic interfacial layer of paramagnetic oxide material between paramagnetic and ferromagnetic oxides [19] and ferromagnetism for a topological insulator (TI) interfacial layer between TI and ferromagnetic oxide [66]. These are the systems, where PNR was used as a unique probe to explore and understand such emerging phenomena at the interfaces. Recently, NR technique, due to its intrinsic strength in deciphering different isotope and interface magnetism, has played an important role in revealing the interfacial structure and magnetic phases as well as its coupling in different heterostructures.

6 Summary

In summary, the specular NR technique is discussed with both unpolarized and polarized modes and its successful use for the investigation of emerging phenomena at interfaces of both soft (biophysical and soft matter) and hard (magnetism) condensed matter physics. It is fair to stress that neutron reflectivity, due to its inherent sensitivity to reveal small nuclear and magnetic structure with sub-nanometer depth resolution, has been and will continue to play a unique and major role in this exciting research area of thin films and heterostructures.

References

[1] A.O. Adeyeye, G. Shimon, Chapter 1 - Growth and Characterization of Magnetic Thin Film and Nanostructures, in: R.E. Camley, Z. Celinski, R.L. Stamps (Eds.) Handbook of Surface Science, North-Holland 2015, pp. 1-41.

[2] B.P. Toperverg, H. Zabel, Neutron scattering in nanomagnetism, in: F. Fernandez-Alonso, D.L. Price (Eds.) Neutron scattering—magnetic and quantum phenomena, Experimental Methods in the Physical Sciences, Academic Press 2015, pp. 339-434.

[3] D. Zang, Y. Tarasevich, L. Zhang, S. Tarafdar, C. Ding, Self-Assembled and Artificial Surfaces/Interfaces: From Soft Matter to Metamaterials, Advances in Condensed Matter Physics, 2018 (2018) 9701423.

[4] S. Singh, M. Swain, S. Basu, Kinetics of interface alloy phase formation at nanometer length scale in ultra-thin films: X-ray and polarized neutron reflectometry, Progress in Materials Science, 96 (2018) 1-50.

[5] C.F. Majkrzak, Neutron scattering studies of magnetic thin films and multilayers, Physica B: Condensed Matter, 221 (1996) 342-356.

[6] M.R. Fitzsimmons, C. Majkrzak, Modern Techniques for Characterizing Magnetic Materials,, Springer, New York2005.
[7] S.K. Sinha, E.B. Sirota, S. Garoff, H.B. Stanley, X-ray and neutron scattering from rough surfaces, Physical Review B, 38 (1988) 2297-2311.
[8] A.J. Dianoux, G.H. Lander, Neutron Data Booklet, Old City 2002.
[9] S. Singh, S. Basu, P. Bhatt, A.K. Poswal, Kinetics of alloy formation at the interfaces in a Ni-Ti multilayer: X-ray and neutron reflectometry study, Physical Review B, 79 (2009) 195435.
[10] S. Singh, S. Basu, M. Gupta, C.F. Majkrzak, P.A. Kienzle, Growth kinetics of intermetallic alloy phase at the interfaces of a Ni/Al multilayer using polarized neutron and x-ray reflectometry, Physical Review B, 81 (2010) 235413.
[11] C. Carelli, R.N. Young, R.A.L. Jones, M. Sferrazza, The contrast match neutron reflectivity technique for the study of broad polymer/polymer interfaces, Nuclear Instruments and Methods in Physics Research Section B: Beam Interactions with Materials and Atoms, 248 (2006) 170-174.
[12] T. Widmann, L.P. Kreuzer, G. Mangiapia, M. Haese, H. Frielinghaus, P. Müller-Buschbaum, 3D printed spherical environmental chamber for neutron reflectometry and grazing-incidence small-angle neutron scattering experiments, Review of Scientific Instruments, 91 (2020) 113903.
[13] J. Penfold, Neutron reflectivity and soft condensed matter, Current Opinion in Colloid & Interface Science, 7 (2002) 139-147.
[14] S. Singh, H. Bhatt, Y. Kumar, C.L. Prajapat, A. Mishra, S. Bedanta, S. Basu, Interface-driven static and dynamic magnetic properties of ultrathin Fe/Ge multilayers, Applied Surface Science, 570 (2021) 151193.
[15] S. Singh, M.R. Fitzsimmons, T. Lookman, J.D. Thompson, H. Jeen, A. Biswas, M.A. Roldan, M. Varela, Magnetic Nonuniformity and Thermal Hysteresis of Magnetism in a Manganite Thin Film, Physical Review Letters, 108 (2012) 077207.
[16] S. Singh, J.T. Haraldsen, J. Xiong, E.M. Choi, P. Lu, D. Yi, X.D. Wen, J. Liu, H. Wang, Z. Bi, P. Yu, M.R. Fitzsimmons, J.L. MacManus-Driscoll, R. Ramesh, A.V. Balatsky, J.-X. Zhu, Q.X. Jia, Induced Magnetization in $La_{0.7}Sr_{0.3}MnO_3/BiFeO_3$ Superlattices, Physical Review Letters, 113 (2014) 047204.
[17] N. Banu, S. Singh, B. Satpati, A. Roy, S. Basu, P. Chakraborty, H.C.P. Movva, V. Lauter, B.N. Dev, Evidence of Formation of Superdense Nonmagnetic Cobalt, Scientific Reports, 7 (2017) 41856.
[18] M.A. Basha, C.L. Prajapat, H. Bhatt, Y. Kumar, M. Gupta, C.J. Kinane, J.F.K. Cooper, A. Caruana, M.R. Gonal, S. Langridge, S. Basu, S. Singh, Helical magnetic structure and exchange bias across the compensation temperature of Gd/Co multilayers, Journal of Applied Physics, 128 (2020) 103901.
[19] H. Bhatt, Y. Kumar, C.L. Prajapat, C.J. Kinane, A. Caruana, S. Langridge, S. Basu, S. Singh, Emergent Interfacial Ferromagnetism and Exchange Bias Effect in Paramagnetic/Ferromagnetic Oxide Heterostructures, Advanced Materials Interfaces, 7 (2020) 2001172.
[20] J.M. Reynolds, V. Nunez, A.T. Boothroyd, R. Somekh, D.G. Bucknall, S. Langridge, Polarised neutron reflectometry studies of flux penetration in superconducting Nb, Physica B: Condensed Matter, 241-243 (1997) 1104-1106.
[21] C.L. Prajapat, S. Singh, A. Paul, D. Bhattacharya, M.R. Singh, S. Mattauch, G. Ravikumar, S. Basu, Superconductivity-induced magnetization depletion in a ferromagnet through an insulator in a ferromagnet–insulator–superconductor hybrid oxide heterostructure, Nanoscale, 8 (2016) 10188-10197.
[22] S. Singh, H. Bhatt, Y. Kumar, C.L. Prajapat, B. Satpati, C.J. Kinane, S. Langridge, G. Ravikumar, S. Basu, Superconductivity-driven negative interfacial magnetization in $YBa_2Cu_3O_{7-\delta}/SrTiO_3/La_{0.67}Sr_{0.33}MnO_3$ heterostructures, Applied Physics Letters, 116 (2020) 022406.

[23] Y. Kumar, H. Bhatt, C.L. Prajapat, A.P. Singh, F. Singh, C.J. Kinane, S. Langridge, S. Basu, S. Singh, Suppression of the superconducting proximity effect in ferromagnetic-superconducting oxide heterostructures with ion-irradiation, Journal of Applied Physics, 129 (2021) 163902.
[24] H. Bhatt, Y. Kumar, C.L. Prajapat, C.J. Kinane, A. Caruana, S. Langridge, S. Basu, S. Singh, Correlation of Magnetic and Superconducting Properties with the Strength of the Magnetic Proximity Effect in $La_{0.67}Sr_{0.33}MnO_3/SrTiO_3/YBa_2Cu_3O_{7-\delta}$ Heterostructures, ACS Applied Materials & Interfaces, 14 (2022) 8565-8574.
[25] S. Krueger, Neutron reflection from interfaces with biological and biomimetic materials, Current Opinion in Colloid & Interface Science, 6 (2001) 111-117.
[26] A. Tummino, E. Scoppola, G. Fragneto, P. Gutfreund, A. Maestro, R.A.W. Dryfe, Neutron reflectometry study of the interface between two immiscible electrolyte solutions: Effects of electrolyte concentration, applied electric field, and lipid adsorption, Electrochimica Acta, 384 (2021) 138336.
[27] W. Lu, J. Zhang, J. Xu, X. Wu, L. Chen, In Situ Visualized Cathode Electrolyte Interphase on LiCoO2 in High Voltage Cycling, ACS Applied Materials & Interfaces, 9 (2017) 19313-19318.
[28] J. Penfold, R.K. Thomas, The application of the specular reflection of neutrons to the study of surfaces and interfaces, Journal of Physics: Condensed Matter, 2 (1990) 1369-1412.
[29] T.H. Laby, R.T.W. Bingham, The reflection and diffraction of X-rays, Proceedings of the Royal Society of London. Series A, Containing Papers of a Mathematical and Physical Character, 133 (1931) 274-291.
[30] E. Fermi, W. Zinn, Reflection of neutrons on mirrors., Phys. Rev., 70 (1946) 103A.
[31] G.P. Felcher, R.O. Hilleke, R.K. Crawford, J. Haumann, R. Kleb, G. Ostrowski, Polarized neutron reflectometer: A new instrument to measure magnetic depth profiles, Review of Scientific Instruments, 58 (1987) 609-619.
[32] J. Lekner, Theory of reflection of electromagnetic and particle waves. , Martinus Nijhoff Publishers,1987.
[33] V.F. Sears, Fundamental aspects of neutron optics, Physics Reports, 82 (1982) 1-29.
[34] H. Zabel, X-ray and neutron scattering at thin films, in: U. Rössler (Ed.) Festkörperprobleme 30: Plenary Lectures of the Divisions Semiconductor Physics Thin Films Dynamics and Statistical Physics Magnetism Metal Physics Surface Physics Low Temperature Physics Molecular Physics of the German Physical Society (DPG), Regensburg, March 26 to 30, 1990, Springer Berlin Heidelberg, Berlin, Heidelberg, 1990, pp. 197-217.
[35] S.J. Blundell, J.A.C. Bland, Polarized neutron reflection as a probe of magnetic films and multilayers, Physical Review B, 46 (1992) 3391-3400.
[36] L.G. Parratt, Surface Studies of Solids by Total Reflection of X-Rays, Physical Review, 95 (1954) 359-369.
[37] L. Névot, P. Croce, Caractérisation des surfaces par réflexion rasante de rayons X. Application à l'étude du polissage de quelques verres silicates, Rev. Phys. Appl. (Paris), 15 (1980) 761-779.
[38] A.R. Rennie, http://www.reflectometry.net/reflect.htm#Analysis.
[39] S. Basu, S. Singh, A new polarized neutron reflectometer at Dhruva for specular and off-specular neutron reflectivity studies, Journal of Neutron Research, 14 (2006) 109-120.
[40] S. Singh, D. Bhattacharya, S. Basu, Specular and off-specular polarized neutron reflectivity at Dhruva, Neutron News, 25 (2014) 31-33.
[41] Z. Fisher, A. Jackson, A. Kovalevsky, E. Oksanen, H. Wacklin, Chapter 1 - Biological Structures, in: F. Fernandez-Alonso, D.L. Price (Eds.) Experimental Methods in the Physical Sciences, Academic Press2017, pp. 1-75.
[42] S. Mitragotri, D.G. Anderson, X. Chen, E.K. Chow, D. Ho, A.V. Kabanov, J.M. Karp, K. Kataoka, C.A. Mirkin, S.H. Petrosko, J. Shi, M.M. Stevens, S. Sun, S. Teoh, S.S. Venkatraman, Y. Xia, S. Wang, Z. Gu, C. Xu, Accelerating the Translation of Nanomaterials in Biomedicine, ACS Nano, 9 (2015) 6644-6654.

[43] K. Simons, M.J. Gerl, Revitalizing membrane rafts: new tools and insights, Nature Reviews Molecular Cell Biology, 11 (2010) 688-699.
[44] P.L. Yèagle, Lipid regulation of cell membrane structure and function, The FASEB Journal, 3 (1989) 1833-1842.
[45] G. Fragneto, Neutrons and model membranes, The European Physical Journal Special Topics, 213 (2012) 327-342.
[46] G. Fragneto, R. Delhom, L. Joly, E. Scoppola, Neutrons and model membranes: Moving towards complexity, Current Opinion in Colloid & Interface Science, 38 (2018) 108-121.
[47] G. Fragneto, T. Charitat, F. Graner, K. Mecke, L. Perino-Gallice, E. Bellet-Amalric, A fluid floating bilayer, Europhys. Lett., 53 (2001) 100-106.
[48] A.R. Mazzer, L.A. Clifton, T. Perevozchikova, P.D. Butler, C.J. Roberts, D.G. Bracewell, Neutron reflectivity measurement of protein A–antibody complex at the solid-liquid interface, Journal of Chromatography A, 1499 (2017) 118-131.
[49] A. Martel, L. Antony, Y. Gerelli, L. Porcar, A. Fluitt, K. Hoffmann, I. Kiesel, M. Vivaudou, G. Fragneto, J.J. de Pablo, Membrane Permeation versus Amyloidogenicity: A Multitechnique Study of Islet Amyloid Polypeptide Interaction with Model Membranes, Journal of the American Chemical Society, 139 (2017) 137-148.
[50] N. Banu, S. Singh, S. Basu, A. Roy, H.C.P. Movva, V. Lauter, B. Satpati, B.N. Dev, High density nonmagnetic cobalt in thin films, Nanotechnology, 29 (2018) 195703.
[51] M.A. Basha, C.L. Prajapat, M. Gupta, H. Bhatt, Y. Kumar, S.K. Ghosh, V. Karki, S. Basu, S. Singh, Interface induced magnetic properties of Gd/Co heterostructures, Physical Chemistry Chemical Physics, 20 (2018) 21580-21589.
[52] S. Singh, M.A. Basha, H. Bhatt, Y. Kumar, M. Gupta, Interface morphology driven exchange interaction and magnetization reversal in a Gd/Co multilayer, Physical Chemistry Chemical Physics, 24 (2022) 6580-6589.
[53] J. Hoppler, J. Stahn, C. Niedermayer, V.K. Malik, H. Bouyanfif, A.J. Drew, M. Rössle, A. Buzdin, G. Cristiani, H.U. Habermeier, B. Keimer, C. Bernhard, Giant superconductivity-induced modulation of the ferromagnetic magnetization in a cuprate–manganite superlattice, Nature Materials, 8 (2009) 315-319.
[54] D.K. Satapathy, M.A. Uribe-Laverde, I. Marozau, V.K. Malik, S. Das, T. Wagner, C. Marcelot, J. Stahn, S. Brück, A. Rühm, S. Macke, T. Tietze, E. Goering, A. Frañó, J.H. Kim, M. Wu, E. Benckiser, B. Keimer, A. Devishvili, B.P. Toperverg, M. Merz, P. Nagel, S. Schuppler, C. Bernhard, Magnetic Proximity Effect in $YBa_2Cu_3O_7/La_{2/3}Ca_{1/3}MnO_3$ and $YBa_2Cu_3O_7/LaMnO_{3+\delta}$ Superlattices, Physical Review Letters, 108 (2012) 197201.
[55] P. Yu, J.S. Lee, S. Okamoto, M.D. Rossell, M. Huijben, C.H. Yang, Q. He, J.X. Zhang, S.Y. Yang, M.J. Lee, Q.M. Ramasse, R. Erni, Y.H. Chu, D.A. Arena, C.C. Kao, L.W. Martin, R. Ramesh, Interface Ferromagnetism and Orbital Reconstruction in $BiFeO_3$-$La_{0.7}Sr_{0.3}MnO_3$ Heterostructures, Physical Review Letters, 105 (2010) 027201.
[56] S. Singh, J. Xiong, A.P. Chen, M.R. Fitzsimmons, Q.X. Jia, Field-dependent magnetization of $BiFeO_3$ in an ultrathin $La_{0.7}Sr_{0.3}MnO_3/BiFeO_3$ superlattice, Physical Review B, 92 (2015) 224405.
[57] P. Jain, Q. Wang, M. Roldan, A. Glavic, V. Lauter, C. Urban, Z. Bi, T. Ahmed, J. Zhu, M. Varela, Q.X. Jia, M.R. Fitzsimmons, Synthetic magnetoelectric coupling in a nanocomposite multiferroic, Scientific Reports, 5 (2015) 9089.
[58] C.L. Prajapat, H. Bhatt, Y. Kumar, T.V.C. Rao, P.K. Mishra, G. Ravikumar, C.J. Kinane, B. Satpati, A. Caruana, S. Langridge, S. Basu, S. Singh, Interface-Induced Magnetization and Exchange Bias in LSMO/BFO Multiferroic Heterostructures, ACS Applied Electronic Materials, 2 (2020) 2629-2637.
[59] J. Wang, J.B. Neaton, H. Zheng, V. Nagarajan, S.B. Ogale, B. Liu, D. Viehland, V. Vaithyanathan, D.G. Schlom, U.V. Waghmare, N.A. Spaldin, K.M. Rabe, M. Wuttig, R. Ramesh, Epitaxial BiFeO3 Multiferroic Thin Film Heterostructures, Science, 299 (2003) 1719-1722.

[60] C. Ederer, N.A. Spaldin, Weak ferromagnetism and magnetoelectric coupling in bismuth ferrite, Physical Review B, 71 (2005) 060401.
[61] C. He, A.J. Grutter, M. Gu, N.D. Browning, Y. Takamura, B.J. Kirby, J.A. Borchers, J.W. Kim, M.R. Fitzsimmons, X. Zhai, V.V. Mehta, F.J. Wong, Y. Suzuki, Interfacial Ferromagnetism and Exchange Bias in $CaRuO_3/CaMnO_3$ Superlattices, Physical Review Letters, 109 (2012) 197202.
[62] T.S. Santos, B.J. Kirby, S. Kumar, S.J. May, J.A. Borchers, B.B. Maranville, J. Zarestky, S.G.E. te Velthuis, J. van den Brink, A. Bhattacharya, Delta Doping of Ferromagnetism in Antiferromagnetic Manganite Superlattices, Physical Review Letters, 107 (2011) 167202.
[63] P.A. Salvador, A.M. Haghiri-Gosnet, B. Mercey, M. Hervieu, B. Raveau, Growth and magnetoresistive properties of $(LaMnO_3)_m(SrMnO_3)_n$ superlattices, Applied Physics Letters, 75 (1999) 2638-2640.
[64] A.J. Grutter, H. Yang, B.J. Kirby, M.R. Fitzsimmons, J.A. Aguiar, N.D. Browning, C.A. Jenkins, E. Arenholz, V.V. Mehta, U.S. Alaan, Y. Suzuki, Interfacial Ferromagnetism in $LaNiO_3/CaMnO_3$ Superlattices, Physical Review Letters, 111 (2013) 087202.
[65] J. Hoffman, I.C. Tung, B.B. Nelson-Cheeseman, M. Liu, J.W. Freeland, A. Bhattacharya, Charge transfer and interfacial magnetism in $(LaNiO_3)_n/(LaMnO_3)_2$ superlattices, Physical Review B, 88 (2013) 144411.
[66] F. Katmis, V. Lauter, F.S. Nogueira, B.A. Assaf, M.E. Jamer, P. Wei, B. Satpati, J.W. Freeland, I. Eremin, D. Heiman, P. Jarillo-Herrero, J.S. Moodera, A high-temperature ferromagnetic topological insulating phase by proximity coupling, Nature, 533 (2016) 513-516.

Neutron Conferences and Workshops

November 2022

Workshop - Perspectives with High Magnetic Fields at Neutron Sources
November 2-4, 2022, Grenoble, France
https://workshops.ill.fr/event/292/overview

Workshop - Powder Diffraction Workshop 2022
November 3-5, 2022, Lucas Heights, Australia
https://www.ansto.gov.au/whats-on/powder-diffraction-workshop-2022

Conference - AANSS2022 | ANBUG-AINSE Neutron Scattering Symposium
November 9-11, 2022, ANSTO, Australia
https://www.ansto.gov.au/whats-on/aanss2022-anbug-ainse-neutron-scattering-symposium

Seminar - UK Neutron Scattering Group Early Career Meeting
November 10-11, 2022, Oxford, UK
https://iop.eventsair.com/nsg2022/

Seminar - JDN2022: Neutron, Diffraction@ESS, Spectroscopy and Modelling
November 14-17, 2022, Biarritz, France
https://jdn-conference.net/

XIX School on Neutrons as Probes of Condensed Matter
November 14-19, 2022, BARC, Mumbai, India
https://www.csr.res.in/news/NPCM2022_Flyer.pdf

Workshop - SAS2022: ANSTO Small Angle Scattering Workshop
November 15-17, 2022, Lucas Heights, Australia
https://www.ansto.gov.au/whats-on/sas2022-ansto-small-angle-scattering-workshop

Workshop - Workshop on Topology in Magnetic Materials
November 22-24, 2022, Herzberg, Switzerland
https://indico.psi.ch/event/12550/

December 2022

Workshop - 6th Neutron and Muon School at J-PARC MLF and JRR-3
December 12-16, 2022, Tokai, Ibaraki, Japan
https://mlfinfo.jp/sp/school/6th-nms/index.html

Conference - ICXRNO 2022: 16. International Conference on X-Ray and Neutron Optics
December 29-30, 2022, Vienna, Austria
https://waset.org/x-ray-and-neutron-optics-conference-in-december-2022-in-vienna

January 2023

Workshop - Winter School of SANS Data Analysis
January 9-13, 2023, Oak Ridge National Laboratory, United States
https://conference.sns.gov/event/358/

Conference - ICRANP 2023: International Conference on Recent Advances in Neutron Physics
January 09-10, 2023 in Tokyo, Japan
https://waset.org/recent-advances-in-neutron-physics-conference-in-january-2023-in-tokyo

February 2023

Workshop - HERCULES 2023 - HERCULES European School 2023: Neutrons & Synchrotron Radiation for Science
18 Feb 2023 - 31 Mar 2023, Grenoble, France
https://hercules-school.eu/

Workshop - ISIS Neutron Training Course 2023
February 28 – March 9, 2022, ISIS, UK
https://www.isis.stfc.ac.uk/Pages/ISIS-Neutron-Training-Course.aspx

March 2023

Conference - Neutron and the X-ray Scattering in Materials Science symposium at the TMS 2023
March 19-23, 2023, San Diego, California, United States
https://www.tms.org/AnnualMeeting/TMS2023

Conference - ECNS 2023: Eighth European Conference on Neutron Scattering,
Mar 20-23, 2023, Garching, Germany
https://indico.frm2.tum.de/event/263/

April 2023

Seminar - Neutron scattering enabled energy materials design at MRS Spring Meeting April 10-14, 2023, San Francisco, United States
https://www.mrs.org/meetings-events/spring-meetings-exhibits/2023-mrs-spring-meeting/call-for-papers/detail/2023_mrs_spring_meeting/ch03/Symposium_CH03

May 2023

Conference - ICNO 2024: International Conference on Neutron Optics
May 13-14, 2023, Amsterdam, Netherlands
https://waset.org/neutron-optics-conference-in-may-2023-in-amsterdam

Conference - ICXRNO 2023: International Conference on X-Ray and Neutron Optics
May 11-12, 2023, Sydney, Australia
https://waset.org/x-ray-and-neutron-optics-conference-in-may-2023-in-sydney

June 2023

Seminar - Gordon Research Seminar - Neutron Scattering
June 24-25, 2023, Ventura, CA, United States
https://www.grc.org/neutron-scattering-grs-conference/2023/

Conference - Gordon Research Conference - Neutron Scattering for a Sustainable Society
June 25-30, 2023, Ventura, CA, United States
https://www.grc.org/neutron-scattering-conference/2023/

August 2023

Conference - ICNPNS 2023: International Conference on Neutron Physics and Neutron Scattering
August 03-04, 2023, Montreal, Canada
https://waset.org/neutron-physics-and-neutron-scattering-conference-in-august-2023-in-montreal

September 2023

Conference - ICNPNS 2023: International Conference on Neutron Physics and Neutron Scattering
September 20-21, 2023, Lisbon, Portugal
https://waset.org/neutron-physics-and-neutron-scattering-conference-%20in-september-2023-in-lisbon

November 2023

Conference - AOCNS 2023: Asia-Oceania Conference on Neutron Scattering
November 13–18, 2023, Royal Garden Hotel, Dongguan, China
http://aonsa.org/aocns/

Workshop - 8th European Crystallography School 2023
June 18-24, 2023, Helmholtz-Zentrum Berlin, Germany
https://www.helmholtz-berlin.de/events/ecs8/index_en.html

Neutron Scattering Society of India

(Registered No. Maharashtra State, Mumbai, 2011 GBBSD/1696)

(For Promotion of Neutron Scattering Research in India)

C/o Solid State Physics Division,
Bhabha Atomic Research Centre, Mumbai 400085

Phones: 91-22-25595376, 25593754, 25594307
Email:neutron@barc.gov.in; URL: http://www.**nssi.org.in**

Affix your PP size recent photograph here

*Application Form for Membership**

Name (in Capital letters)[$]: Prof/Dr/Ms/Mr **(Surname last)**	
Nationality:	**Date of Birth:** (dd/mm/yyyy)
Academic Qualification:	**Sex: M/F**
Profession:	**Neutron User Experience** (in yrs):
Nature of Present work:	
Affiliation: **Pin Code:**	**Residential Address:** **Pin Code:**
STD Code & Phone (O):	**STD Code & Phone (R):**
STD Code & FAX No.	**Mobile:**
Email-1:	**Email-2:**
[+]Details of Cheque/DD[+]: No.	**dated** **Bank:**
Endorsed by: (Either an existing member of NSSI or Head of the Affiliated Institute/University)	
Name & Designation	**Signature**
Date:	**Signature:**

*Life Membership fee: Rs. 1000/- (One thousand only)

[+]In favour of 'Neutron Scattering Society of India' payable at Mumbai

To: Secretary, ***Neutron Scattering Society of India***